GFZ
Helmholtz-Zentrum
POTSDAM

Originally published as:

Ivandic, M., Juhlin, C., Lueth, S., Bergmann, P., Kashubin, A., Sopher, D., Ivanova, A., Baumann, G., Henninges, J.(2015): Geophysical monitoring at the Ketzin pilot site for CO2 storage: New insights into the plume evolution. - *International Journal of Greenhouse Gas Control*, *32*, p. 90-105.

DOI: http://doi.org/10.1016/j.ijggc.2014.10.015

Geophysical monitoring at the Ketzin pilot site for CO_2 storage: New insights into the plume evolution

M. Ivandic[1*] (monika.ivandic@geo.uu.se), C. Juhlin[1](christopher.juhlin@geo.uu.se), S. Lüth[2] (slueth@gfz-potsdam.de), P. Bergmann[2] (bergmann@gfz-potsdam.de), A. Kashubin[3] (AKashubin@slb.com), D. Sopher[1] (daniel.sopher@geo.uu.se), A. Ivanova[2] (aivanova@gfz-potsdam.de), G. Baumann[2] (baumann@gfz-potsdam.de) and J. Henninges[2] (jan.henninges@gfz-potsdam.de)

[1] Uppsala University, Department of Earth Sciences, Villavägen 16, 75236, Uppsala, Sweden.
[2] GFZ German Research Centre for Geosciences, Helmholtz Centre Potsdam, Telegrafenberg, 14473 Potsdam, Germany.
[3] WesternGeco, Schlumberger House, Buckingham Gate, Gatwick, West Sussex, RH6 0NZ, England.

*Corresponding author: tel: +46 72 7068 484, fax: +46 18 501 110

Abstract

To date, 3D time-lapse seismic monitoring at the Ketzin CO_2 storage pilot site comprised a baseline survey conducted in 2005 and two repeat surveys conducted in 2009 and 2012. At the time of the first repeat survey (22–25 kt of CO_2), the CO_2 plume was found to be concentrated around the injection well with a maximum lateral extent of approximately 300–400 m and a thickness of 5–20 m. Data from the 2012 survey (61 kt of CO_2), show further growth and migration of the amplitude anomaly interpreted to be induced by the CO_2 injection. The anomaly is similar in shape to that obtained from the 2009 survey, but significantly stronger and larger by ~ 150 m in the N-S direction and by ~ 200 m in the E-W direction. In agreement with the 2009 survey, the new data show a westward propagation of the plume, a trend governed by the complex structure of the reservoir. No evidence of systematic changes in the seismic signature within the overburden is observed. A quantitative assessment of the plume reveals a 15% discrepancy with the injected amount, which could be attributed to the ongoing dissolution processes. However, the estimated quantity also contains significant uncertainty.

Keywords: CO_2 sequestration, Ketzin pilot site, Seismic monitoring, 3D time-lapse (4D)

1. Introduction

The CO_2 storage site at Ketzin near Berlin, Germany, has been developed to advance the scientific understanding of how to geologically store CO_2 and to investigate the processes of underground CO_2 injection and migration (Förster et al., 2006; Martens et al., 2013). Injection of CO_2 at the site began in June 2008 and ended in August 2013. During the five-year period, about 67,000 tons of CO_2 were injected through the CO2 Ktzi 201/2007 well over the depth interval 630–650 m into sandstone layers on the southern flank of a gently dipping anticline in the North German Basin. Three observation wells—CO2 Ktzi 200/2007 and CO2 Ktzi 202/2007, drilled in 2007 prior to injection, and CO2 Ktzi 203/2012, drilled in 2012—have been used to observe the injection process and to monitor the movement of CO_2 in the storage formation (Fig. 1).

The extensive monitoring program, which consists of geological, geophysical, and geochemical investigations, is capable of detecting CO_2 on different scales. Various geophysical methods, such as 2D and 3D surface seismic surveys (Bergmann et al., 2011; Ivanova et al., 2012; Ivandic et al., 2012), crosswell surveys (Zhang et al., 2012), and moving source profiling (Yang et al., 2010), have already successfully imaged the movement of the injected CO_2 within the target reservoir zone at the Ketzin storage site. Among them, the 3D time-lapse reflection seismic method has proven to be the most effective tool for mapping the spatial extent of the CO_2 injected at the Ketzin site as well as for its quantitative analysis. The method has already been used successfully for both qualitative and quantitative monitoring at other saline-aquifer CO_2 storage sites, such as the Sleipner project site (Arts et al., 2002; Chadwick et al., 2005).

The 3D seismic survey acquired in the fall of 2005 prior to CO_2 injection provided information about the geometry of the reservoir and its overburden (Juhlin et al., 2007) and served as a baseline for later surveys conducted to accurately model key reservoir changes caused by the subsequent injection of CO_2.

In previous investigations, the CO_2 signature could be detected by increased reflectivity at the top of the target reservoir, by a change in attenuation, and by a reduced propagation velocity within the reservoir (Lüth et al., 2011). Results from the first 3D repeat survey, conducted in the fall of 2009 while between 22 to 25 kt of CO_2 had been injected, showed that the CO_2 plume was concentrated around the injection well; at that time, the plume had a lateral extent of approximately 300–400 m and a thickness of about 5–20 m (Ivanova et al., 2012). The obtained time-lapse seismic signature was interpreted as being caused by fluid saturation changes only. Later modeling of the AVO/AVA response indicated that pressure has a rather minor impact on the seismic amplitudes at the Ketzin site (Ivanova et al., 2013b). The 4D seismic signature, results from petrophysical measurements on reservoir core samples, and repeated pulsed neutron-gamma (PNG) logging of CO_2 saturation levels enabled quantification of the amount of CO_2 in the reservoir. Approximately 93%–95% of the injected CO_2 was interpreted to have been imaged by the first repeat 3D seismic data (Ivanova et al., 2012).

In the summer and fall of 2012, when about 61 kt of CO_2 had been injected, a second 3D repeat seismic survey was acquired over an area of about 10 km^2, approximately 3 km^2 more than that of the first repeat survey and some 4 km^2 less than that of the baseline survey (Fig. 1). The acquisition and processing of this latest dataset followed the same scheme as in the previous two surveys to ensure maximum repeatability of the 4D surveys carried out over time.

Here we present results from data processing and time-lapse analysis of the second 3D repeat dataset collected three years after the first 3D repeat survey and with a further 39 kt of additional CO_2 stored in the target reservoir. Maps of the areal extent of the amplitude anomaly and traveltime delays reveal the new migration pathways of the injected CO_2 and allow us to quantify the growth of the CO_2 plume since the time of the first 3D repeat survey.

2. Reservoir and caprock properties

The target saline aquifer, the Stuttgart Formation (Fig. 2), is lithologically heterogeneous both laterally and vertically. It consists of a complex geometric arrangement of sandstone and siltstone interbedded with mudstone; therefore, the spatial distribution of reservoir properties also varies. The primary target for CO_2 storage is in the upper part of the Stuttgart Formation, situated at a depth of 630–650 m, where the main sandstone units (9–20 m thick) display a typical channel facies with effective porosities in the range of 20%–25% (Förster et al. 2010). Individual sandstone bodies may be stacked together to form channel belts. The possible heterogeneous distribution of reservoir bodies in the Stuttgart Formation was also indicated by higher amplitude features on the summed absolute amplitude map, generated over a time window covering the Stuttgart Formation (Juhlin et al., 2007). The general northeast-southwest trend of these amplitude anomalies is consistent with the expected general orientation of the sandy channels. Continuous wavelet transform analysis of the baseline dataset also indicated that the reservoir was heterogeneous and suggested the presence of meandering channel facies within it (Kazemeini et al., 2009).

The immediate overlying caprock of the Stuttgart Formation is the Weser Formation, which mainly consists of clayey and sandy siltstone alternating with carbonate and evaporite horizons (Beutler and Nitsch, 2005). The top of the Weser Formation contains a 10–20-m thick anhydrite layer, known as the Heldburg-Gips or K2 horizon, which is a prominent seismic reflector throughout the entire survey area (Juhlin et al., 2007). The top of the anhydrite lies about 80 m above the top of the Stuttgart Formation. The Weser Formation is overlain by mud/clay-carbonates of the Arnstadt Formation, which exhibits similar sealing properties (Beutler and Nitsch, 2005). Above the Arnstadt Formation, Lower Jurassic shallow-water sandstones at depths of 250–400 m have been used for natural gas storage. These sandstones together with interlayered mudstone, siltstone, and anhydrite form a multilayered system of saline aquifers. The overlying seal for this aquifer system is the approximately 80-m thick Tertiary Rupelian claystone unit, which separates the groundwater horizons above from the deep saline aquifers below. Together with the anticlinal structure, this multibarrier system ensures safe and responsible long-term storage. The near-surface layers are mainly composed of Quaternary sands and tills, which exhibit a relatively flat surface topography.

The pressure and temperature of the Stuttgart Formation control the phase state of injected CO_2. At the CO_2 injection depth the Stuttgart Formation exhibits pressure and temperature conditions that cause CO_2 to be in gaseous state near the critical point. Given the thermodynamic conditions present in the injection well, CO_2 is entering the formation in the supercritical state and is undergoing phase transition towards the

gaseous state within a short distance from the wellbore. Kazemeini et al. (2010) showed that replacing the saline brine by CO_2 in a gaseous state causes a significant change in fluid acoustic properties.

3. Acquisition of the second repeat 3D dataset

The second 3D repeat survey followed the same template acquisition scheme (Table 1) and used identical recording equipment, source (an accelerated EWGIII weight drop (Yordkayhun et al., 2009)), and acquisition parameters as in the baseline 3D survey (Juhlin et al., 2007) and the first 3D repeat survey (Ivanova et al., 2012). Templates were numbered in the same way as in the previous two surveys, with an origin in the lower left-hand corner of the survey area. The second 3D repeat survey area initially consisted of 33 templates, but two of them (T3:5 and T2:5), located in the southeastern corner of the survey area (Fig. 3), were skipped due to wet conditions that could have caused considerable delays in the survey and extensive property damage. Because the CO_2 plume propagation trend was mainly westward, the area of the two skipped templates was considered to be of lower priority.

Acquisition of the second 3D repeat survey began September 4, 2012, and proceeded through the templates in a snake-like manner to cover approximately a 10-km^2 area around the injection site and ended October 30, 2012. A total of 5445 source points were recorded during the 48 days of active acquisition. To enhance the signal strength each source point generally consisted of eight hits with the weight drop, that were later stacked using a diversity stacking method.

Source and receiver coordinates were re-surveyed according to the specifications of the baseline survey (Juhlin et al., 2007). The new positions were generally located within a few decimeters of the baseline point coordinates. Five receiver lines made up one swath. When a template was moved in the receiver line direction within a swath, half of the stations remained in the current template to be a part of the active spread in the next template. A similar overlapping scheme was used between the source points of adjacent swaths. This overlap of source points and recording stations from template to template yielded a nominal fold of 25 for the survey area. However, due to logistical constraints from roads, villages, and inaccessible infrastructure, particularly at the injection site, there are some areas in which only a reduced fold was achieved (Fig. 4).

For the second repeat survey, receivers could be planted at nearly all locations, including the injection site, which in the 2005 and 2009 surveys was very sparsely covered due to the infrastructure near the wells, resulting in very low fold for some CDP bins in that area (Juhlin et al., 2007). Those receiver points, however, are excluded from the data processing flow for the time-lapse analysis in this work.

In comparison with the previous surveys, there is a considerable shotpoint gap in the 2012 survey northeast of the injection site due to a solar panel facility that has recently expanded. Those source and receiver stations that were affected by the new solar panels and by a new sand pit to the north of the survey area showed larger lateral and vertical position errors in the 2012 survey than in the 2009 survey.

The overall position error was substantially larger for the source locations (14.3% differed from the 2005 locations by more than 0.6 m and 6.6% differed by more than 1.0 m) than for the receiver locations (7.3% of the receiver locations differed by more than 0.6 m and only 0.7% by more than 1.0 m). These changes also affected station elevations. Relative to the 2009 data, there are many more source and receiver stations in the 2012 survey with elevation changes exceeding 0.6 m (6.6% of receivers and 12.8% of sources). However, the relative time-shifts between the surveys were corrected using trace-to-trace crosscorrelations, tying the repeat survey to the baseline survey and considerably reducing the 4D noise that could arise from these changes (see Section 4).

4. Seismic data processing

Because the baseline and repeat datasets were to be compared in a time-lapse analysis, the same data processing workflow and parameters used in the previous surveys (Juhlin et al., 2007; Ivanova et al., 2012) were applied here. To maximize repeatability in fold and azimuthal coverage for the time-lapse analysis, the datasets were limited to the baseline and repeat data subsets that contain common traces. The data processing workflow is described in detail in Juhlin et al. (2007) and the main parameters are summarized in Table 2. An example of a common shot gather from the baseline survey and the second repeat survey processed prior to normal moveout (NMO) correction is displayed in Fig. 5, showing good repeatability of

the two datasets (NRMS = 0.3-0.5). A comparison of the amplitude spectra of the two datasets also shows a similar energy content at all frequencies (Fig. 6).

Owing to the different weather and ground conditions during the surveys, static shifts had to be recalculated. Kashubin et al. (2011) showed that the static time shifts at the Ketzin site strongly correlate with the soil-moisture saturation, which in turn depends on cumulative precipitation at the location prior to data acquisition. Therefore, new calculations of the static corrections were necessary to accommodate the changes in the near-surface conditions.

Unlike in previous surveys, where static time shifts were derived from the first arrivals and applied within the individual time-lapse surveys, a different static correction approach was used here, in which trace-to-trace time shifts of the time-lapse datasets were determined from crosscorrelation (Bergmann et al., 2011). The relative time-lapse differences (TLDs) in reflection arrival times between the baseline and repeat survey trace pairs were derived automatically, decomposed in a surface-consistent manner, and applied to the repeat data to tie them to the baseline data to accommodate for static differences between them.

Aside from being time-efficient, as it does not require labor-intensive and time-consuming first-break picking, the crosscorrelation workflow has proven to be quicker and more accurate, exhibiting less time-lapse noise and, thus, enhancing the CO_2-induced time-lapse signature (Bergmann et al., 2012). Fig. 7 shows the effect of the pre-stack TLD static correction on the time-delay distribution. The maps show the decomposed values in geographic coordinates.

Differences in survey geometry, processing, and near-surface velocities during data acquisition can reduce the repeatability of a monitor survey, altering the phase, amplitude, and static solution between surveys. The objective of 4D seismic acquisition and processing is to minimize differences in the seismic data that are unrelated to injection or production, while preserving differences that are due to reservoir processes. Although the 3D seismic campaigns at the Ketzin site were acquired with the same equipment and during the same seasons and were processed in a consistent manner from pre-stack to post-stack, certain differences in phase, amplitudes, and time shifts remained, most likely due to nonrepeatable ambient noise and changes in environmental conditions. Therefore, to minimize these and obtain the actual injection-related changes, the seismic volumes underwent further cross calibration.

Cross-equalization of post-stack seismic datasets typically includes bandwidth and phase equalization to compensate for different source wavelets, and amplitude balancing to scale the data to the same amplitude (or energy) level (Rickett and Lumley, 2001). The cross-equalized trace is calculated by convolving the input trace with the estimated wavelet operator, to shape and match the reflection data of one survey to another (Ross et al., 1996). Design of the matching filters uses a window above the reservoir, where no change is expected. This was verified by testing different calibration windows above the reservoir zone, which all lead to same time-lapse results. The crosscalibration process followed the same workflow and used the same parameters as in both the sparse 3D seismic data processing (Ivandic et al., 2012) and cross-equalization of the first 3D repeat seismic data to the baseline data (Ivanova et al., 2012). That is, the data were first calibrated to match in phase and time, followed by phase and frequency shaping by filtering, crossnormalization, and time-variant shifting using Hampson-Russell's Pro4D software. Difference sections obtained by subtracting the two datasets after each step of the cross-equalization processing workflow show an enhancement of the time-lapse reservoir signal and suppression of differences caused by other factors.

5. Stacked and migrated volumes and time-lapse results

The stacked and migrated subvolume of the second 3D repeat dataset provides, as in the previous two surveys, good-quality images of the subsurface in the time interval from 150 ms to about 900 ms. The most prominent event in the migrated subvolume, the reflection from the 20-m thick anhydrite layer at the top of the Weser Formation (K2 horizon), is highlighted in Fig. 8. The base of the target Stuttgart Formation lies about 80 ms below the K2 horizon.

Fig. 9 and Fig. 10 show final migrated stacked sections from the baseline and the second repeat datasets. Presented are inline 1167 and crossline 1098, both located in the vicinity of the injection borehole where the time-lapse effects are expected to be most prominent. The area around the target reservoir is marked with a yellow rectangle (top at 480 ms, bottom at 560 ms). A comparison of the stacked sections from the two surveys reveals changes in amplitudes within the Stuttgart Formation at approximately 530 ms, near the injection borehole in both the inline and crossline images. The observed stronger reflections in the target area are interpreted to be due to the presence of injected CO_2. The CO_2 should enhance the impedance contrast of the internal layers in the aquifer (Kazemeini et al., 2010).

The quality of the seismic match between the two time-lapse processed volumes after cross-equalization was assessed using the normalized root mean square (NRMS) difference, a commonly used metric that measures the relative difference between two traces and is sensitive to differences in timing, phase, and amplitudes (Kragh and Christie, 2002). The map of the NRMS values for the crosscalibrated seismic subvolumes shows quite good repeatability with NRMS errors in the range of 0.2–0.4 over most of the area (Fig. 11). Typical values for modern 4D surveys are 0.1 to 0.4, which represent an ability to reproduce seismic amplitudes to within 10-40% in the final stacked data (Miller and Helgerud, 2009). Larger NRMS deviations at the edges of the survey area are due to lower fold there and, consequently, lower signal-to-noise ratio. Higher NRMS values (> 0.6) in the area around the injection well are due to injection-related reservoir changes and the locally reduced fold (Fig. 4).

The two crosscalibrated seismic datasets were then differenced, and the amplitude differences near the top of the reservoir, which are likely related to injection effects, were analyzed in terms of CO_2 plume evolution. To remove time-lapse effects unrelated to the CO_2 injection, the amplitude differences were normalized to the peak amplitude of the K2 reflection.

6. Assessment of CO_2 plume migration

Time-lapse analysis of the first repeat 3D seismic survey (following injection of 22–25 kt of CO_2) revealed a pronounced amplitude anomaly. This anomaly, with a lateral extent of 300–400 m and a thickness of 5–20 m, was situated at the top of the reservoir near the injection well (Fig. 12a). The irregular pattern of this anomaly, attributed to the injected CO_2, was seen as an indicator of the variable permeability and strong lateral heterogeneity of the reservoir. Other seismic features on the timeslice with amplitudes ranging up to about 0.25 were attributed to remaining non-repeatable noise, as they are present throughout the entire survey area. Therefore, the white contour at 0.3 represents the outline of the CO_2 plume at the time of the survey.

Subtraction of the cross-equalized second repeat dataset from the baseline survey revealed that the CO_2-induced anomaly has expanded since the time of the first repeat survey in 2009 (Fig. 12b). The amplitude differences at the reservoir level indicate that the CO_2 plume has grown by 150 m in the N-S direction and 200 m in the W-E direction. It is similar in shape to the plume from 2009, but has a stronger amplitude, with the maximum located 60–100 m north-northwest of the injection well. The westward propagation of the plume observed in the first repeat dataset is persistent. The complex geometry of the sandstone bodies within the reservoir can also be the cause for the small-scale heterogeneities in the CO_2 distribution pattern, especially prominent east of the injection site.

Fig. 13 and Fig. 14 show vertical cross sections along inline 1170 and crossline 1093. They both are located close to the injection site and show a prominent time-lapse signature at approximately 42 ms below the K2 reflector, corresponding to the top of the Stuttgart Formation. Lower fold in this area resulted in poorer images of the near-surface structure here (Juhlin et al., 2007; Fig. 9 and Fig 10 this paper), and, consequently, in a somewhat higher level of 4D noise at shallower levels.

In principle, migration of CO_2 upward through the overburden, particularly in the gas phase, can be detected on seismic data by the generation of distinct high amplitude reflections of localized extent (“bright spots”) caused by the sharp decrease in acoustic impedance within rocks saturated by CO_2 (Chadwick et al., 2009). Because no such time-lapse anomalies have been observed above the reservoir layer in the vicinity of the injection site, there is no indication of upward migration of CO_2 into the caprock.

7. Evaluation of CO_2 saturations

The quantitative analysis of the CO_2 plume imaged by the first 3D repeat seismic data was performed using CO_2 saturations determined from PNG logging (Ivanova et al., 2012). PNG logging is frequently used for saturation evaluation in oil and gas fields (e.g. Smolen 1996; Morris et al. 2005), and has also been used successfully for CO_2 monitoring in saline aquifers (Müller et al., 2007; Murray et al., 2010). At Ketzin, it has been used for monitoring in-situ saturation changes at the borehole scale. Following the approach of our previous study (Ivanova et al., 2012), saturation conditions for the first repeat 3D seismic survey have now been reevaluated on the basis of refined input parameters, and results from the PNG logs acquired during the second 3D seismic survey are presented.

PNG tools radiometrically measure the thermal neutron macroscopic capture cross section Σ, which is derived from the decay of capture gamma ray flux with time from thermal neutron capture processes, typically dominated by the presence of chlorine in brine. The high Σ contrast between brine and CO_2 results in a high sensitivity to saturation changes. In time-lapse mode, changes of saturation S can be calculated from the Σ change between baseline and a repeat logging run, and the Σ difference of the involved pore fluids alone (e.g. Ellis and Singer, 2007):

$$S_{w,base} - S_{w,\log} = \frac{\Sigma_{base} - \Sigma_{\log}}{\varphi (\Sigma_w - \Sigma_g)}, \quad (1)$$

where the subscripts *log* and *base* refer to the repeat and baseline logging runs, and φ is formation porosity (total porosity derived from open-hole logging data after Norden et al. (2010). For the current application, the subscripts *w* and *g* correspond to the considered pore fluids brine and CO_2, and the CO_2 saturation is equal to the change in brine saturation, $S_{w,base}$ - $S_{w,log}$. A revised Σ_w value of 97.6 capture units (c.u.: Baumann, 2013) was used, based on the chemical composition of the formation brine from the Ketzin site (Würdemann et al., 2010), and a Σ_g value of 0.014 c.u. (Baumann, 2013), corresponding to conditions close to the critical point of CO_2 .

This standard approach is based on the assumption of a simple displacement process, whereby the injected CO_2 displaces the brine originally present within the formation. Because of the mutual solubility between water and CO_2, further processes such as evaporation and salt precipitation can occur, especially in the direct vicinity of an injection well. Similar effects are known to occur during gas production (Kleinitz et al., 2003), and have been predicted for CO_2 injection on the basis of numerical simulations (Pruess and García, 2002). Similar simulations have also been performed specifically for conditions representative for the Ketzin site (Muller et al., 2009). The effects of evaporation and salt precipitation were here additionally taken into account using an extended PNG saturation model (Baumann et al., 2014) for the Ktzi 201 injection well.

At Ketzin, a total of six PNG repeat logging runs have been performed since the start of injection in June 2008. Analogous to the approach in Ivanova et al. (2012), the results from the second (June 2009) and third (March 2010) PNG repeat runs were averaged to obtain results representative for the time of the first 3D seismic repeat survey in October 2009. For the second 3D seismic repeat survey, the results from the sixth PNG run performed in October 2012 were used.

Fig. 15 shows the measured Σ formation logs and the calculated CO_2 saturations using the standard (displacement) PNG model for all wells and the results of the extended model for the Ktzi 201 injection well. It should be noted that the Σ formation curves are partially affected by gas-filled well annuli during the repeat logging runs, causing an offset from the baseline logs. Affected log sections occur both above (mainly in Ktzi 201 and Ktzi 202) and below (Ktzi 202) the main reservoir intervals.

Saturation changes mainly occur within the porous and permeable reservoir sandstone intervals. For the time of the first 3D seismic repeat survey, corresponding to the second and third PNG repeats, saturation changes also occur in the siltstone and sandstone layer underlying the main reservoir sandstones in the Ktzi 201 injection well. At the sixth PNG repeat, a decreased thickness of the interval containing CO_2 can be observed, with increasing saturations within the upper reservoir intervals. This is consistent with the injection regime, as injection rates after the third PNG repeat were mainly about 50% lower than before, and the sixth PNG repeat was additionally recorded during a shut-in period of several months duration.

For the extended PNG saturation model, more variable CO_2 saturation profiles with a general tendency toward higher saturation values compared to the standard displacement model were calculated in the upper injection intervals. Since there is strong evidence from the PNG logging data for such effects to occur but no independent observations for them have existed until now, results from both models have been considered. Therefore, a set of minimum and maximum saturation values for the reservoir intervals are presented here. On the basis of lithological information, a number of individual sections were defined for each well (compare black bars in Fig. 15) for which average CO_2 saturations were calculated.

Table 3 contains the average CO_2 saturations calculated as weighted arithmetic mean values over the intervals containing CO_2 and the geometries of the averaged intervals.

8. Quantification of the growing CO_2 plume and consideration of uncertainties

Monitoring and verification of the stored CO_2 visible in time-lapse geophysical data is important to assess the integrity of the storage site and to monitor potential leakage (JafarGandomi and Curtis, 2013). Chadwick et al. (2005) demonstrated that the 4D seismic technique can provide a reasonable estimate of the in situ mass of CO_2, but that complete verification is not possible due to a number of uncertainties.

Quantitative analysis of the first 3D repeat time-lapse seismic data from the Ketzin site was performed and showed a close agreement with the actual injected amount of CO_2 (Ivanova et al., 2012), but, as in the Sleipner case (Chadwick et al., 2005), a number of uncertainties were also acknowledged that could significantly influence the estimation. Although the method integrates the 4D seismic signature, petrophysical analysis on core samples, and in-situ CO_2 saturations obtained from PNG logging, it retains several uncertainties that are conditioned by inherent assumptions and simplifications, the complex structure of the reservoir, and limited knowledge of the formation properties (Ivanova et al., 2012).

Seismic parameters used to estimate the total mass of the CO_2 imaged on the seismic data are the normalized reflection amplitude difference, mapped at the reservoir level, and time delays of reflections from below the injection horizon due to the reduced velocities in the CO_2-saturated rocks ("velocity push-down effect"). In 2009, the time-delays were obtained by manual picking (Ivanova et al., 2012). In this study, they are evaluated using a more robust approach, which consists of performing a crosscorrelation in windows above (at 250–450 ms) and below the reservoir (at 600–800 ms) to estimate the optimal time shifts for each window. The optimal time shift is chosen on the basis of the highest correlation coefficient achieved between the baseline and repeat surveys for a given time shift within the window of interest. The same cross-correlation time-shift analysis approach was used by White et al. (2011; 2013). The difference between these optimal time shifts for the upper and lower windows is then calculated. This is assumed to be representative of the delay that is caused by changes within the reservoir only. Because this approach is data driven, the interpretation is less prone to subjective errors associated with the interpretation when performing manual picking. It also considers the optimal time shift over a window, rather than at a given event, which should also reduce errors compared with the previous method. To make a comparison between the two repeat survey results, the same approach has been applied to the first 3D repeat dataset (Fig. 16).

In both 3D seismic repeat data sets, the lowest time delay values found within the amplitude anomaly area are in a range of 1.4–1.6 ms, which is within the noise level of 1–2 ms (1.2–2.4 m). Therefore, those values have been tested as a lower cutoff limit of the delays that are due to the injected CO_2. Similarly, since the normalized amplitude differences in the areas not reached by the CO_2 range up to 0.3, this value was used as the cutoff value for amplitude differences used in the mass estimation. CO_2 saturation values were then assigned to each CDP bin using the same empirical approach as Ivanova et al. (2012)—i.e. by converting the normalized time-lapse amplitude differences (Fig. 12a and Fig. 12b) to saturations using the saturations obtained from PNG logging for calibration. Both the time-delays (Fig. 16a and Fig. 16b) and the saturations obtained from the amplitude differences were used as a basis for the CO_2 mass estimation approach described in Arts et al. (2002):

$$M=\Sigma_N \rho\cdot\varphi\cdot S_{CO_2}\cdot dx\cdot dy\cdot H \tag{2}$$

where

$$H=\Delta T\cdot\frac{V_1\cdot V_2}{2\cdot\left|V_1-V_2\right|} \tag{3}$$

where

H	thickness of the layer containing CO_2
ρ	CO_2 density
φ	porosity of the reservoir
S_{CO2}	CO_2 saturation in the reservoir
dx, dy	inline and crossline spacing
N	total number of CDPs
ΔT	time-delay (velocity push-down effect)
V_1	velocity in brine saturated reservoir
V_2	velocity in CO_2 saturated reservoir (at saturation S_{CO2}).

A CO_2 density of 215 kg/m^3 obtained from the NIST database (Lemmon et al., 2001) and an average reservoir porosity of 20%, taken from Förster et al. (2010), were assumed to be the same in all CDP bins.

Because seismic velocities from the reservoir are not available, except the Vp velocity baseline from cross-hole measurements, Vp velocities used in equation (3) were obtained from petrophysical experiments on two core samples from the target reservoir (Kummerow and Spangenberg, 2011; Ivanova et al., 2012). Frequency dispersion was ignored, because it was not considered to be large enough to affect the mass of CO_2 in the estimation (Ivanova et al., 2012). The velocity of 3135 m/s obtained from ultra-sonic laboratory experiments with 100% formation brine saturation was used for the pre-injection velocity in the reservoir. This value is close to the one observed in the baseline cross-hole seismic data (Zhang et al., 2012), confirming that the error that could arise from using the petrophysical results in equation (3) is probably small. Moreover, since equation (3) uses the velocity difference between brine saturated samples and those containing CO_2, the potential discrepancy should be even smaller.

In the petrophysical experiments on core samples saturated with CO_2, Vp velocities were calibrated with corresponding values of CO_2 saturation obtained from the electrical resistivity petrophysical experiment. Once calibrated, the Vp velocities were linearly interpolated in Ivanova et al. (2013a) resulting in the following relationship between Vp and CO_2 saturation (standard deviation is - 187 m/s):

$$\frac{\Delta Vp}{Vp} = -0.46 \times S_{CO_2}. \quad (4)$$

The thickness distribution of the layer saturated with CO_2 in equation (3) corresponds to the distribution of time-delays and varies from 10 m to 30 m.

The mass estimates were first made for each bin and then summed to give the total mass imaged by the seismic data. The difference between the reevaluated minimum and maximum saturation scenarios (Table 3) is significantly less than in Ivanova et al. (2012), resulting in nearly the same estimated quantities. Fig. 17a and Fig. 17b show the resulting CO_2 mass distribution maps for both 3D seismic repeat surveys for the time-delay cutoff of 1.5 ms, which gives an estimate for the 2009 data that is in agreement with those reported by Ivanova et al. (2012). It was, therefore, selected here as a reference cutoff for comparison with the estimates for 2012 and for further analysis of the impact on the estimated quantities as a result of variations in the input reservoir properties.

The discrepancy between the amount injected at the time of the first repeat survey and the amount observed in the seismic data is within 3%–5%. However, the estimates obtained for the 2012 data show an about a 15% difference between the two values. On the basis of reservoir and geochemical simulations (Kempka and Kühn, 2013; Kempka et al., 2013), this discrepancy can be entirely attributed to the loss of the CO_2 due to dissolution during four years of injection. However, considering the uncertainties related to the choice of the cutoff values and the reservoir model, it is more likely that the mismatch between the actual injected amount and the estimated one is even larger than 15%. That is, the estimated mass is strongly sensitive to the choice of the time-delay cutoff. For example, an increment of only 0.1 ms results in a 5–7 kt change of mass. In comparison to the time-delay cutoff impact, the choice of the amplitude cutoff plays a minor role here—i.e. a change in the lower amplitude limit of 0.1 results only in about a 1–1.5 kt difference. The impact of the reservoir model uncertainties was also tested. At 1% higher reservoir porosity the estimated CO_2 mass would be greater by 2.5 kt. The same effect on the estimates would have 10 kg/m^3 higher CO_2 density. The results for both 3D repeat datasets are summarized in Table 4.

The results demonstrate that small changes in input values can have a significant impact on the estimated quantities. Therefore, considering the complexity of the Stuttgart Formation, the simplified reservoir model with constant reservoir porosity and CO_2 density used here may induce considerable errors in the mass estimate. In addition, despite the fact that we have rather good information about temperature conditions at Ketzin from downhole measurement data (Henninges et al., 2011), there is some remaining uncertainty about the exact distribution of the p/T conditions over the extent of the CO_2 plume. Based on the integration of seismic modeling and multiphase fluid flow simulations, it has been shown that reservoir temperature plays an important role in quantitative interpretation of the Ketzin seismic data (Ivanova et al., 2013a).

Since the CO_2 saturation distribution cannot be derived directly from the seismic data, the saturation model was constrained on the basis of the PNG logging data from only three wells. The scarcity of input

data and the empirical approach used to assign CO_2 saturation values to CDP bins resulted in a very simplified saturation distribution within the reservoir.

It is also important to note that there is only a small number of direct petrophysical observations, which, therefore, cannot provide a good statistical basis for the determination of seismic velocities based on CO_2 saturations and that the petrophysical experiments were carried out on samples that are assumed to be representative of the average properties of the whole reservoir (Ivanova et al., 2012).

Finally, the vertical resolution of the seismic data poses another limitation on the mass estimation—i.e. CO_2 saturated layers in which the thickness is beneath the limit of seismic detectability, as in the outer parts of the spreading plume, cannot be imaged and, therefore, quantified using the tools presented here. To overcome this shortfall, further seismic forward modeling with realistic signal-noise ratios and different saturation scenarios incorporated into the model data would need to be performed.

9. Conclusions

The second 3D monitor seismic survey at the Ketzin CO_2 storage site was acquired in the late summer/early fall 2012 to map the CO_2 plume evolution since the last monitor survey in 2009, as well as to detect any migration of the injected CO_2 out of the storage reservoir during that period. High repeatability for the new dataset was achieved by following the same acquisition and data processing schemes as in the previous two surveys. The only difference in the processing workflow was the application of a recently implemented time-lapse static correction approach.

Subtraction of the cross-equalized second repeat dataset from its respective baseline dataset provided new insights into how the plume has developed through time. The seismic reflection amplitude difference map reveals that the CO_2 plume has expanded since the time of the first repeat survey in 2009. The migration of the injected CO_2 shows a similar heterogeneous pattern to that observed at the time of the first repeat survey, but larger by approximately 150 m in the N-S direction and 200 m in the W-E direction. The amplitudes are significantly stronger with the highest amplitudes located at approximately 80 m north-northwest of the injection well. The westward component of plume propagation observed in the first repeat survey is now more pronounced, confirming the strong lateral heterogeneity of the Stuttgart Formation. There is no indication of upward migration of CO_2 into the caprock. Quantification of the time shifts associated with CO_2 emplacement has been achieved using correlation coefficients calculated within windows above and below the reservoir. This method is considered to be less subjective and more accurate compared to manual picking. Based on the 4D time shifts below the reservoir, inferences similar to those based on the amplitude anomaly can be made about the evolution of the CO_2 plume. The time shift anomaly is similar in shape and lateral extent to the amplitude anomaly.

Changes in the seismic signature, petrophysical measurements on core samples, and geophysical logging of CO_2 saturation levels, allow the amount of CO_2 imaged by the seismic data to be estimated and compared to the actual injected quantity. The estimates performed on the first 3D seismic repeat dataset show consistency between the in situ CO_2 mass and the actual amount injected at the time of the survey. Although the shortfall in the imaged 2012 amounts can, in principle, be explained by the ongoing dissolution processes, significant uncertainties, attributed mainly to the limited vertical resolution of the seismic data, the heterogeneous reservoir composition at the site and a limited knowledge about the distribution of its properties, remain.

The results presented here demonstrate that the size and location of the CO_2 plume can be clearly delimited qualitatively with seismic data. However, it is also clear that the quantification of the volume of injected CO_2 from the 4D seismic response is uncertain due to the significant uncertainty in key reservoir and seismic parameters.

Acknowledgements

The second 3D repeat survey was conducted within the CO_2MAN collaborative project, which has been facilitating research and development work at the pilot site and has been funded by the Federal Ministry for Education and Research and the industry partners VNG, RWE Power AG, Vattenfall, Statoil Petroleum AS, Dillinger Hüttenwerke, Saarstahl AG, and OMV Exploration and Production GmbH. GLOBE ClaritasTM, under license from the Institute of Geological and Nuclear Sciences Limited, Lower Hutt, New Zealand, was used to process the seismic data. Hampson and Russell (CGG Veritas) provided Pro4D for the time-

lapse analysis. This is Geotechnologien paper number GEOTECH-2167. We are grateful to Phil Christie, Patrick Smith, John Wood, and Samantha Perkins of Schlumberger for their input to an early version of the manuscript and two anonymous reviewers for their constructive criticism. D. Sopher was funded by the Swedish Research Council (project number 2010-3657).

References

Arts, R., Elsayed, R. , van der Meer, L., Eiken, O., Ostmo, S., Chadwick, A., Kirby, G., Zinszner, B., 2002. Estimation of the mass of injected CO_2 at Sleipner using time-lapse seismic data: 64th Annual International Conference and Exhibition, EAGE, Extended Abstracts, H16.

Baumann, G., Henninges, J., De Lucia, M., 2014. Monitoring of saturation changes and salt precipitation during CO_2 injection using pulsed neutron-gamma logging at the Ketzin site. Intl J Greenhouse Gas Control 28, 134-146.

Bergmann P., Yang, C., Lüth, S., Juhlin. C., Cosma, C., 2011. Time-lapse processing of 2D seismic profiles with testing of static correction methods at the CO_2 injection site Ketzin (Germany). Journal of Applied Geophysics 75, 124–139.

Bergmann, P., Kashubin, A., Ivandic, M., Juhlin, C., Lüth, S., Ivanova, A., Lundberg, E., Zhang, F., 2012. Cross-correlation time-lapse static corrections versus refraction static corrections on 4D land seismic CO_2 monitoring at Ketzin, Germany. SEG Technical Program Expanded Abstracts 2012: pp. 1–5, doi: 10.1190/segam2012-0686.1.

Beutler, G., Nitsch, E., 2005. Paläographischer Überblick, in G. Beutler, N. Hauschke, E. Nitsch, and U. Vath, eds., Stratigraphie von Deutschland IV, Keuper: Courier Forschungsinstitut Senckenberg, 253, 15–30.

Chadwick, R.A., Arts, R., Eiken, O., 2005. 4D seismic quantification of a growing CO_2 plume at Sleipner, North Sea. In: Dore, A.G. and Vining, B. (eds), Petroleum Geology: North West Europe and Global Perspectives - Proceedings of the 6th Petroleum Geology Conference, Published by the Geological Society, London, 1385–1399.

Chadwick, R.A., Arts, R., Bentham, M., Eiken, O., Holloway, S., Kirby, G.A., Pearce, J.M., Williamson, J.P., Zweigel, P., 2009. Review of monitoring issues and technologies associated with the long-term underground storage of carbon dioxide: In: Underground gas storage : worldwide experiences and future development in the UK and Europe / edited by D. J. Evans and R. A. Chadwick. London : Geological Society of London (Special publication 313), 257–275.

Ellis, D. V., Singer, J. M., 2007. Well logging for earth scientists, 2nd ed., 692 pp., Springer, Dordrecht.

Förster, A., Norden, B., Zinck-Jørgensen, K., Frykman, P., Kulenkampff, J., Spangenberg, E., Erzinger, J., Zimmer, M., Kopp, J., Borm, G., Juhlin, C., Cosma, C., Hurter, S., 2006. Baseline characterization of the CO_2SINK geological storage site at Ketzin, Germany: Environmental Geosciences, 13, 3, 145–161, doi: 10.1306/eg.02080605016.

Förster, A., Schoner, R., Förster, H.J., Norden, B., Blaschke, A.W., Luckert, J., Beutler, G., Gaupp, R., Rhede, D., 2010. Reservoir characterization of a CO_2 storage aquifer: The Upper Triassic Stuttgart Formation in the Northeast German Basin. Mar Petrol Geol 27(10):2156–2172. doi:10.1016/j.marpetgeo.2010.07.010.

Henninges, J., Liebscher, A., Bannach, A., Brandt, W., Hurter, S., Köhler, S., Möller, F., 2011. CO2SINK Group P-T-rho and two-phase fluid conditions with inverted density profile in observation wells at the CO_2 storage site at Ketzin (Germany). Energy Procedia 4, 6085–6090.

Ivandic, M., Yang, C., Lüth, S., Cosma, C., Juhlin, C., 2012. Time-lapse analysis of sparse 3D seismic data from the CO_2 storage pilot site at Ketzin, Germany. Journal of Applied Geophysics, 84, 14–28.

Ivanova, A., Kashubin, A., Juhojuntti, N., Kummerow, J., Henninges, J., Juhlin, C., Lüth, S., Ivandic, M., 2012. Monitoring and volumetric estimation of injected CO_2 using 4D seismic, petrophysical data, core measurements and well logging: a case study at Ketzin, Germany. Geophysical Prospecting, 60, 5, 957–973, doi: 10.1111/j.1365-2478.2012.01045.x.

Ivanova, A., Juhlin, C., Lengler, U., Bergmann, P., Lüth, S., Kempka, T., 2013a. Impact of temperature on CO_2 storage at the Ketzin site based on fluid flow simulations and seismic data. International Journal of Greenhouse Gas Control, doi 10.1016/j.ijggc.2013.05.001.

Ivanova, A., Bergmann, P., Kummerow, J., Yang, C., Lüth, S., Juhlin, C., 2013b. Seismic modeling of the AVO/AVA response to CO_2 injection at the Ketzin site, Germany. Energy Procedia, 40, 490-498, doi: 10.1016/j.egypro.2013.08.056.

JafarGandomi, A., Curtis, A., 2013. Assessing the seismic AVA detectability of CO_2 storage sites using novel time-lapse attributes. Petroleum Geoscience, 19 (4), pp. 357 - 374, doi: dx.doi.org/10.1144/petgeo2012-043

Juhlin C., Giese, R., Zinck-Jørgensen K., Cosma C., Kazemeini, H., Juhojuntti, N., Lüth, S., Norden, B., Förster, A., 2007. 3D baseline seismics at Ketzin, Germany: The CO2SINK project. Geophysics, 72, B121–B132, doi:10.1190/1.2754667.

Kashubin, A., Juhlin, C., Malehmir, A., Lüth, S., Ivanova, A., Juhojuntti, N., 2011. A footprint of rainfall on land seismic data repeatability at the CO_2 storage pilot site, Ketzin, Germany. 81st Annual International Meeting, SEG, Expanded Abstracts, 465–469.

Kazemeini H., Juhlin C., Zinck-Jørgensen K., Norden B. 2009. Application of the continuous wavelet transform on seismic data for mapping of channel deposits and gas detection at the CO2SINK site, Ketzin, Germany. Geophysical Prospecting 57, 111–123.

Kazemeini, S.H., Juhlin, C., Fomel, S., 2010. Monitoring CO_2 response on surface seismic data; a rock physics and seismic modeling feasibility study at the CO_2 sequestration site, Ketzin, Germany. Journal of Applied Geophysics 71 (4), 109–124.

Kempka, T., Kühn, M., 2013. Numerical simulations of CO_2 arrival times and reservoir pressure coincide with observations from the Ketzin pilot site, Germany. Environmental Earth Sciences, Special Issue, 1–11, doi:10.1007/s12665-013-2614-6.

Kempka, T., Klein, E., De Lucia, M., Tillner, E., Kühn, M., 2013. Assessment of long-term CO_2 trapping mechanisms at the Ketzin pilot site (Germany) by coupled numerical modelling. Energy Procedia, Volume 37, 5419–5426, doi:10.1016/j.egypro.2013.06.460.

Kleinitz, W., Dietzsch, G., Köhler, M., 2003. Halite Scale Formation in Gas-Producing Wells. Chemical Engineering Research and Design, 81(3), 352–358, doi: 10.1205/02638760360596900.

Kragh, E., Christie, P., 2002. Seismic repeatability, normalized rms, and predictability. The Leading Edge, 21, 640–647, doi: 10.1190/1.1497316.

Kummerow, J., Spangenberg, E., 2011. Experimental evaluation of the impact of the interactions of CO_2 – SO_2 , brine, and reservoir rock on petrophysical properties: a case study from the Ketzin test site, Germany. Geochemistry, Geophysics, Geosystems 12 (5), 1–10.

Lemmon, E. W., McLinden, M. O., Friend, D. G., 2001. Thermo-physical properties of fluid systems, in P. J. Linstrom and W. G. Mallard, eds., NIST Chemistry WebBook, NIST standard reference database number 69, Gaithersburg, National Institute of Standards and Technology: http://webbook.nist.gov.

Liebscher, A., Martens, S., Möller, F., Kühn, M., 2012. On-shore CO_2 storage in Germany - Experiences gained from the Ketzin pilot site, Brandenburg, the sole German national CO_2 storage project, in: J. Gluyas, and S. Mathias, Geoscience of carbon dioxide (CO_2 storage), Woodhead Publishing Limited.

Lüth, S., Bergmann, P., Cosma, C., Enescu, N., Giese, R., Götz, J., Ivanova, A., Juhlin, C., Kashubin, A., Yang, C., Zhang, F., 2011. Time-lapse seismic surface and down-hole measurements for monitoring CO_2 storage in the CO2SINK project (Ketzin, Germany). Energy Procedia, 4, 3435–3442, doi:10.1016/j.egypro.2011.02.268.

Martens, S., Liebscher, A., Möller, F., Henninges, J., Kempka, T., Lüth, S., Norden, B., Prevedel, B., Szizybalski, A., Zimmer, M., Kühn, M., the Ketzin Group, 2013. CO_2 storage at the Ketzin pilot site, Germany: Fourth year of injection, monitoring, modelling and verification. Energy Procedia, Volume 37, Pages 6434-6443, doi:10.1016/j.egypro.2013.06.573.

Miller, A., Helgerud, M. 2009. 4D seismic repeatability: Lessons from Hoover Madison Marshall. SEG Technical Program Expanded Abstracts 2009. SEG. Chap. 779, p. 3884–3888.

Morris, C., Aswad, T., Morris, F., Quinlan, T., 2005. Reservoir Monitoring with Pulsed Neutron Capture Logs. SPE Europec/EAGE Annual Conference p 16, 94199-MS.

Muller, N., Qi, R., Mackie, E., Pruess, K., Blunt, M. J., 2009. CO_2 injection impairment due to halite precipitation. Energy Procedia, 1(1), 3507–3514, doi: 10.1016/j.egypro.2009.02.143.

Murray, D. R., Yang, X., Horie, T., Yoshimura, T., and Mito, S., 2010. CO_2 Sequestration Monitoring in a Low Salinity Reservoir. Society of Petroleum Engineers. doi:10.2118/130773-MS.

Müller, N., Ramakrishnan, T., Boyd, A., Sakurai, S., 2007. Time-lapse carbon dioxide monitoring with pulsed neutron logging. International Journal of Greenhouse Gas Control, 1, 456–472, doi: 10.1016/S1750-5836(07)00071-0.

Norden, B., Förster, A., Vu-Hoang, D., Marcelis, F., Springer, N., Le Nir, I., 2010. Lithological and petrophysical core-log interpretation in CO_2SINK, The European onshore research storage and verification project. SPE Reservoir Evaluation and Engineering, 13, 179–192, doi: 10.2118/115247-PA.

Pruess, K., García, J., 2002. Multiphase flow dynamics during CO_2 disposal into saline aquifers. Environmenal Geology, 42(2-3), 282–295, doi: 10.1007/s00254-001-0498-3.

Rickett, J. E., Lumley, D. E., 2001. Cross-equalization data processing for time-lapse seismic reservoir monitoring: A case study from the Gulf of Mexico. Geophysics, 66, 1015–1025, doi: 10.1190/1.1487049.

Ross, C. P., Cunningham, G. B., Weber, D. P., 1996. Inside the crossequalization black box. The Leading Edge, 14, 1233–1240.

Smolen, J., 1996. Cased Hole and Production Log Evaluation. Pennwell Publishing Company, Tulsa, Oklahoma.

Soehnel, O., Novotny, P. 1985. Densities of Aqueous Solutions of Inorganic Substances. Elsevier, New York.

D.J. White, 2011. Geophysical monitoring of the Weyburn CO_2 flood: Results during 10 years of injection, Energy Procedia, Vol. 4, p. 3628-3635, ISSN 1876-6102, doi:10.1016/j.egypro.2011.02.293.

White, D. J., 2013. Toward quantitative CO_2 storage estimates from time-lapse 3D seismic travel times: An example from the IEA GHG Weyburn–Midale CO_2 monitoring and storage project, International Journal of Greenhouse Gas Control, vol. 16S, p. S95-S102, doi:10.1016/j.ijggc.2013.01.047.

Würdemann, H., Möller, F., Kühn, M., Heidug, W., Christensen, N. P., Borm, G., Schilling, F. R., the CO2SINK Group, 2010. CO2SINK - From site characterization and risk assessment to monitoring and verification: One year of operational experience with the field laboratory for CO_2 storage at Ketzin, Germany. International Journal of Greenhouse Gas Control, 4(6), 938–951.

Yang, C., Juhlin, C., Enescu, N., Cosma, C., Lüth, S., 2010. Moving source profile data processing, modelling and comparison with 3D surface seismic data at the CO2SINK project site, Ketzin, Germany. Near Surface Geophysics, 8, 601–610.

Yordkayhun, S., Ivanova, A., Giese, R., Juhlin, C., Cosma, C., 2009. Comparison of surface seismic sources at the CO2SINK site, Ketzin, Germany. Geophysical Prospecting, 57, 125-139, doi: 10.1111/j.1365-2478.2008.00737.x.

Zhang, F., Juhlin, C., Cosma, C., Tryggvason, A. Pratt, R. G., 2012. Cross-well seismic waveform tomography for monitoring CO_2 injection: a case study from the Ketzin Site, Germany. Geophysical Journal International, 189: 629–646. doi:10.1111/j.1365-246X.2012.05375.x

Figure Captions

Figure 1. The second repeat 3D survey area (hatched and outlined in blue) with the location of the CO_2 injection well IW (CO2 Ktzi 201/2007) and three observation wells OW1 (CO2 Ktzi 200/2007), OW2 (CO2 Ktzi 200/2007) and OW3 (CO2 Ktzi 203/2007). Black dashed lines outline the baseline 3D survey area and red solid lines the first 3D repeat survey area.

Figure 2. Schematic of the anticline geology at the Ketzin site (after Liebscher et al., 2012). The injection well CO2 Ktzi 201/2007 is marked as Ktzi201. The two observation wells drilled in 2007 are marked as Ktzi200 and Ktzi202, and the observation well drilled in 2012 is Ktzi203. A shallow observation well (P300) has been drilled into the deepest aquifer above the caprock.

Figure 3. The template scheme. The second repeat survey consists of 31 templates that overlap each other by 50%.

Figure 4. CDP fold of the second 3D repeat survey with the same system of inlines and crosslines as in the previous surveys. The injection borehole (IW) is located approximately where inline 1165 and crossline 1100 intersect.

Figure 5. Example of a shot gather from the baseline survey and second repeat survey processed up to Step 16 in Table 2.

Figure 6. Amplitude spectra from the same common source gather location showing a similar frequency content in the baseline data (a) and second repeat data (b).

Figure 7. Delay distributions in baseline-repeat trace pairs before (upper left) and after application of the TLD static correction (upper middle) and evolution of the delays during the decomposition (upper right). Source, receiver, and CDP solutions after surface-consistent decomposition of the delays (lower row).

Figure 8. Cross section of the stacked and migrated subvolume of the second 3D repeat data along crossline 1125 located far from the injection well (see Fig. 4). The K2 horizon (the top Weser Formation highlighted by the white ellipse) is well imaged throughout the entire survey area.

Figure 9. Stacked and migrated subvolumes of the baseline (a) and second 3D repeat data (b) along the inline 1167. The target zone is encompassed by a yellow rectangle, and the time-lapse signature is marked by an arrow. CO_2 marks the location of the injection site on the sections.

Figure 10. Stacked and migrated subvolumes of the baseline (a) and second 3D repeat data (b) along crossline 1098. The target zone is encompassed by a yellow rectangle, and the time-lapse signature is marked by an arrow. CO_2 marks the location of the injection site on the sections.

Figure 11. NRMS map of the baseline and second repeat survey for the crosscalibrated subvolumes in the time interval 100–700 ms. The injection well (IW) is marked by a black dot.

Figure 12. Amplitude difference (baseline – repeat) horizon at the reservoir level normalized to the K2 peak amplitude for the first 3D repeat survey from 2009 (a) and second 3D repeat survey from 2012 (b). The location of the injection well is marked by a black dot and the three observation wells, by gray dots. The white solid contours outline the extent of the CO_2 plume at the time of the two repeat surveys. The contour of the 2009 plume is also shown in (b) (dashed line) to allow for comparison of the CO_2 plume extent between the two surveys.

Figure 13. Time-lapse processing results for the second repeat dataset along inline 1170 that runs nearly over the injection well. Colors highlight the difference between the crosscalibrated subvolumes. Grey rectangle marks the injection well location, with the injection zone at 630–650 m (515–532 ms) marked in yellow. The location of the K2 reflector is shown as a solid black line. The corresponding baseline cross section is shown in the inset (in 100-700 ms time window).

Figure 14. Time-lapse processing results for the second repeat dataset along crossline 1093 that intersects inline 1170 near the injection well. See Fig. 13 caption for legend. The corresponding baseline cross section is shown in the inset (in 100-700 ms time window).

Figure 15. Measured PNG Σ formation (SIGM) log curves of the baseline (B) and second, third, and sixth repeat (R2, R3, R6) logging runs, and calculated CO_2 saturations (Sg) for the displacement (d) and extended (e) PNG saturation models. The first 3D seismic repeat survey (October 2009) is analyzed in conjunction with the logging runs R2 and R3. The second 3D seismic repeat survey (October 2012) is analyzed in conjunction with the logging run R6. Numbers of depth intervals for calculation of average CO_2 volumes and saturations (see Table 3) are indicated with black bars and bold numerals. Lithology after Förster et al. (2010).

Figure 16. Time-delays obtained from differences between the time shifts of the windows above and below the reservoir and used for crosscorrelation of the baseline with the first repeat data (a) and the second repeat data (b). The location of the injection well is marked with a black circle.

Figure 17. Map of CO_2 mass distribution imaged by the first 3D repeat seismic data (a) and second 3D repeat seismic data (b). The injection well Ktzi 201 is marked with a black circle.

Tables and Captions

Parameter	**Value**
Receiver line spacing / number (in one template)	96 m / 5
Receiver station spacing / channels (in one template)	24 m / 48
Source line spacing / number (in one template)	48 m / 12
Source point spacing	24 m or 72 m
CDP bin size	12 m x 12 m
Nominal fold	25
Geophones	28 Hz single
Sampling rate	1 ms
Record length	3s

Source	240 kg accel. weight drop

Table 1. Template acquisition parameters.

Step	Processing Workflow and Parameters
1	Read raw SEGD data
2	Vertical diversity stack
3	Bulk static shift (correction for instrument delay)
4	Extract and apply geometry
5	Trace editing
6	Notch filter: 50 Hz
7	Spherical divergence correction
8	Band-pass filter: 7-14-120-200 Hz
9	Surface consistent deconvolution: 120 ms, gap 16 ms, white noise 0.1%
10	Ground roll mute
11	Spectral equalization: 20-35-80-110 Hz
12	Band-pass filter: 0–300 ms: 15-30-75-115 Hz; 350–570 ms: 14-28-70-110 Hz; 620–1000 ms: 12-25-60-95 Hz
13	Zero-phase filter: converts an average near minimum-phase wavelet of the weight drop source to a wavelet being closer to zero phase
14	Time-lapse difference static correction (with reference to baseline survey)
15	Trace balance using data window
16	NMO
17	Stack
18	Trace balance
19	FX-Decon: inline and crossline directions
20	Trace balance
21	Migration: 3D FD using smoothed stacking velocities

Table 2. Processing workflow for the second 3D repeat dataset

Well	Interval	Top (m)	Bottom (m)	Thickness (m)	Phi (%)	R 2/3		R6	
						Sg min. (%)	Sg max. (%)	Sg min. (%)	Sg max. (%)

201	1	633.75	642.09	8.34	23.5	62.0	65.0	50.0	56.0
	2	642.87	650.99	8.12	25.9	43.5	53.0	15.0	21.0
	3	657.89	661.85	3.96	26.3	17.5	17.5	0	0
	4	661.85	664.11	2.26	27.2	15.0	15.0	0	0
	Average					**42.9**	**47.4**	**32.7**	**38.7**
200	1	634.58	642.24	7.66	27.5	56.5	56.5	58.0	58.0
	2	643.66	649.49	5.83	29.6	14.0	14.0	0	0
	Average					**38.1**	**38.1**	**58.0**	**58.0**
202	1	627.55	631.60	4.05	28.2	40.5	40.5	56.0	56.0

Table 3. Average CO_2 saturations from results of PNG logging for the first and second 3D seismic repeat surveys (PNG repeats R2/3 and R6, respectively), as well as parameters of the averaged intervals in each well.

Density of CO_2 (kg/m^3)		**Reservoir Porosity (%)**	**Time-Delay Cutoff (ms)**	**Amplitude Cutoff**	**Calculated Mass (kt), first repeat data (2009)**	**Calculated Mass (kt), second repeat data (2012)**
2009	**2012**					
266.62	215	20	1.4[a]	0.3	27.4	58.8
266.62	215	20	1.5[a]	0.3	23.4	51.5
266.62	215	20	1.6[a]	0.3	19.8	46.1
255[a]	205[a]	20	1.5	0.3	22.4	49.1
275[a]	225[a]	20	1.5	0.3	24.1	53.9
266.62	215	21[a]	1.5	0.3	24.6	54.0
266.62	215	22[a]	1.5	0.3	25.7	56.6
266.62	215	20	1.5	0.25[a]	23.1	51
266.62	215	20	1.5	0.35[a]	23.7	52.6

[a]Uncertain reservoir parameter

Table 4. Calculated CO_2 mass estimates showing the impact of uncertain reservoir parameters. The actual injected amount of CO_2 was 22–25 kt at the time of the first repeat survey and 61 kt at the time of the second repeat survey.

Figure1

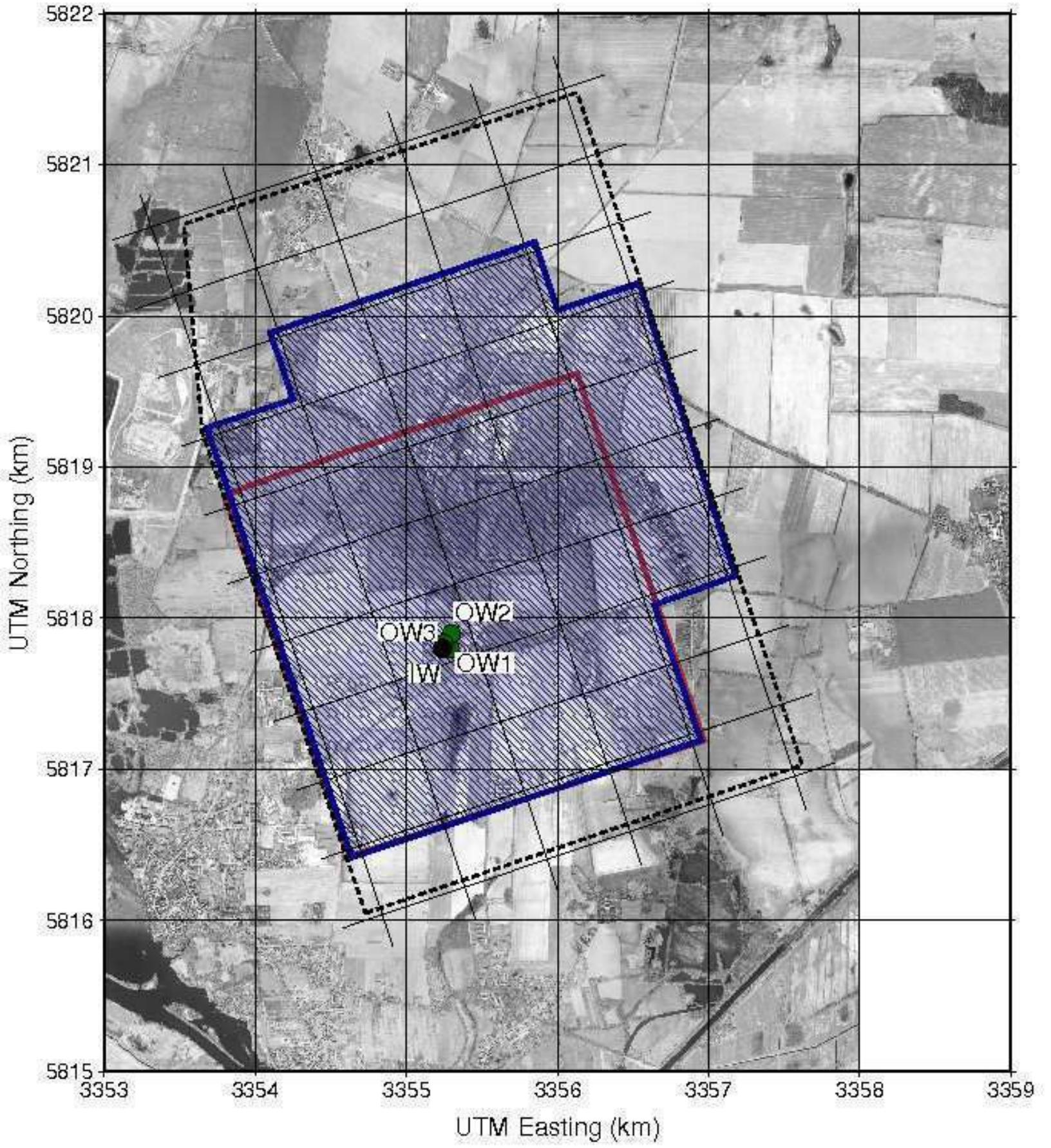
5822
5821
5820
5819
5818
5817
5816
5815
UTM Northing (km)
3353
3354
3355
3356
3357
3358
3359
UTM Easting (km)
OW2
OW3
OW1
IW

Figure2

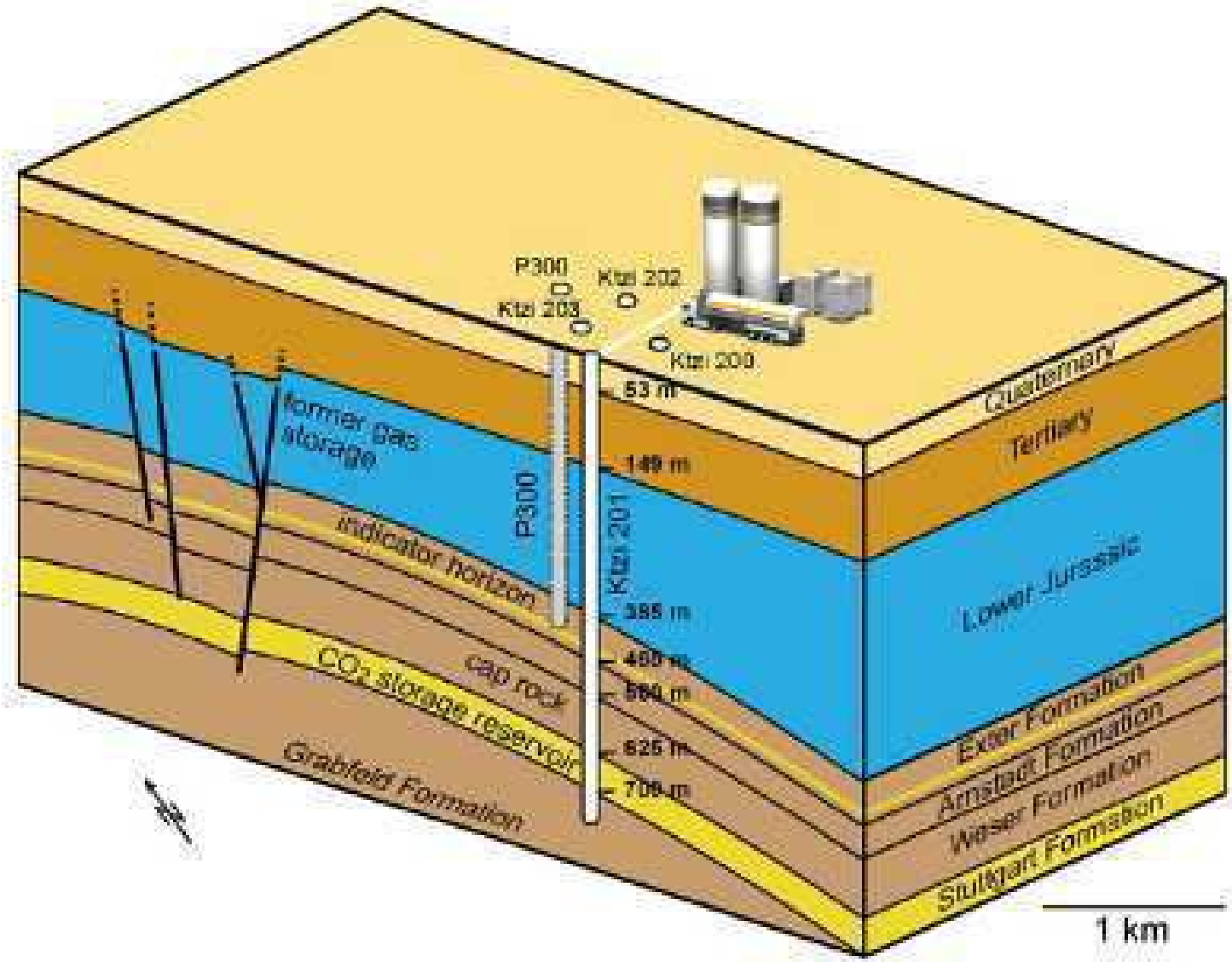
P300
Ktzi 202
Ktzi 203
Ktzi 200
53 m
Quaternary
Tertiary
189 m
former gas storage
P300
Ktzi 201
indicator horizon
385 m
cap rock
CO2 storage reservoir
Lower Jurassic
Exter Formation
Amsbeck Formation
Weser Formation
Stuttgart Formation
Grabfeld Formation
1 km

Figure3

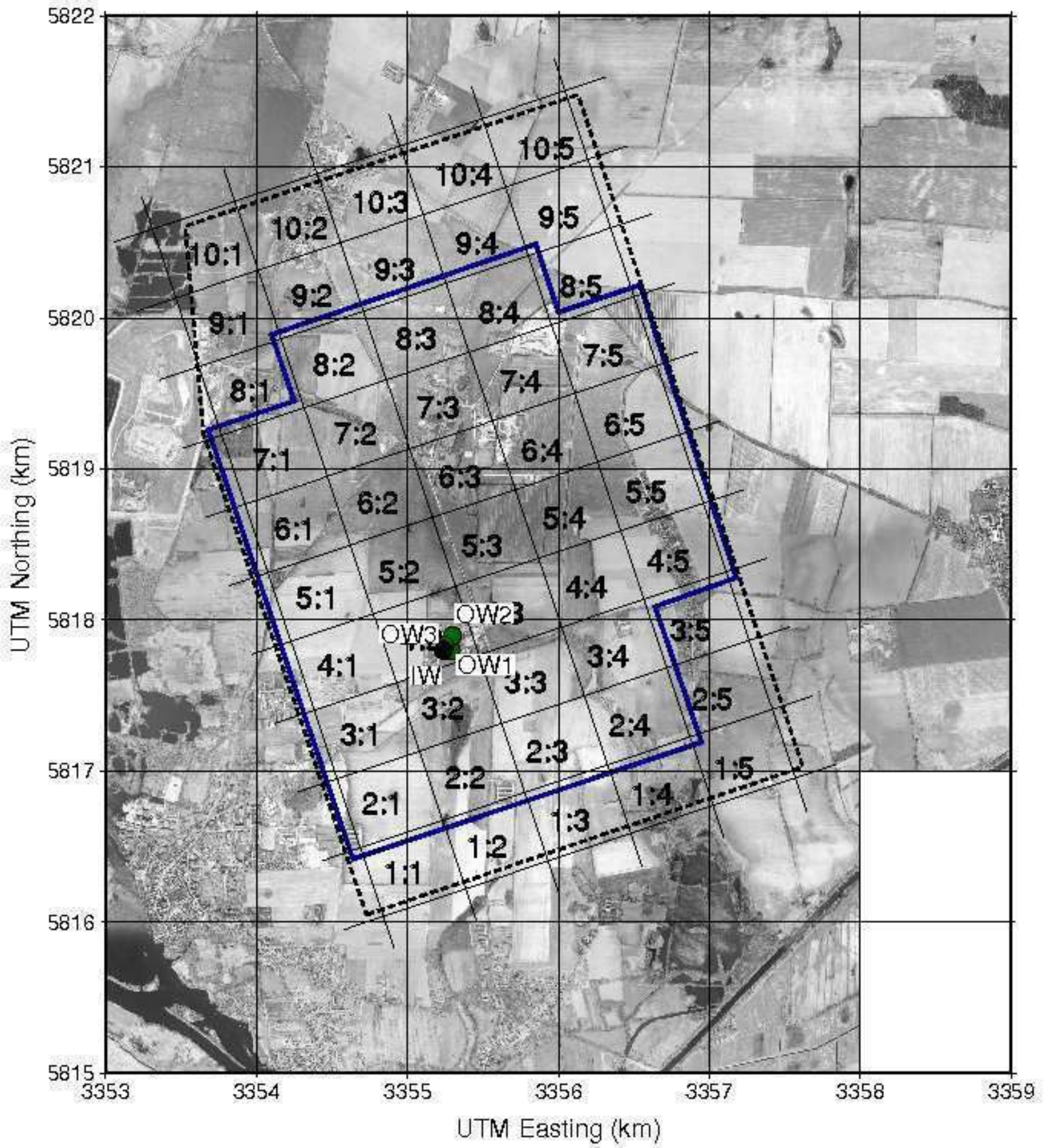
5822
5821
5820
5819
5818
5817
5816
5815
UTM Northing (km)
3353
3354
3355
3356
3357
3358
3359
UTM Easting (km)
10:5
10:4
10:3
10:2
10:1
9:5
9:4
9:3
9:2
9:1
8:5
8:4
8:3
8:2
8:1
7:5
7:4
7:3
7:2
7:1
6:5
6:4
6:3
6:2
6:1
5:5
5:4
5:3
5:2
5:1
4:5
4:4
4:1
3:5
3:4
3:3
3:2
3:1
2:5
2:4
2:3
2:2
2:1
1:5
1:4
1:3
1:2
1:1
OW2
OW3
OW1
IW

Figure4

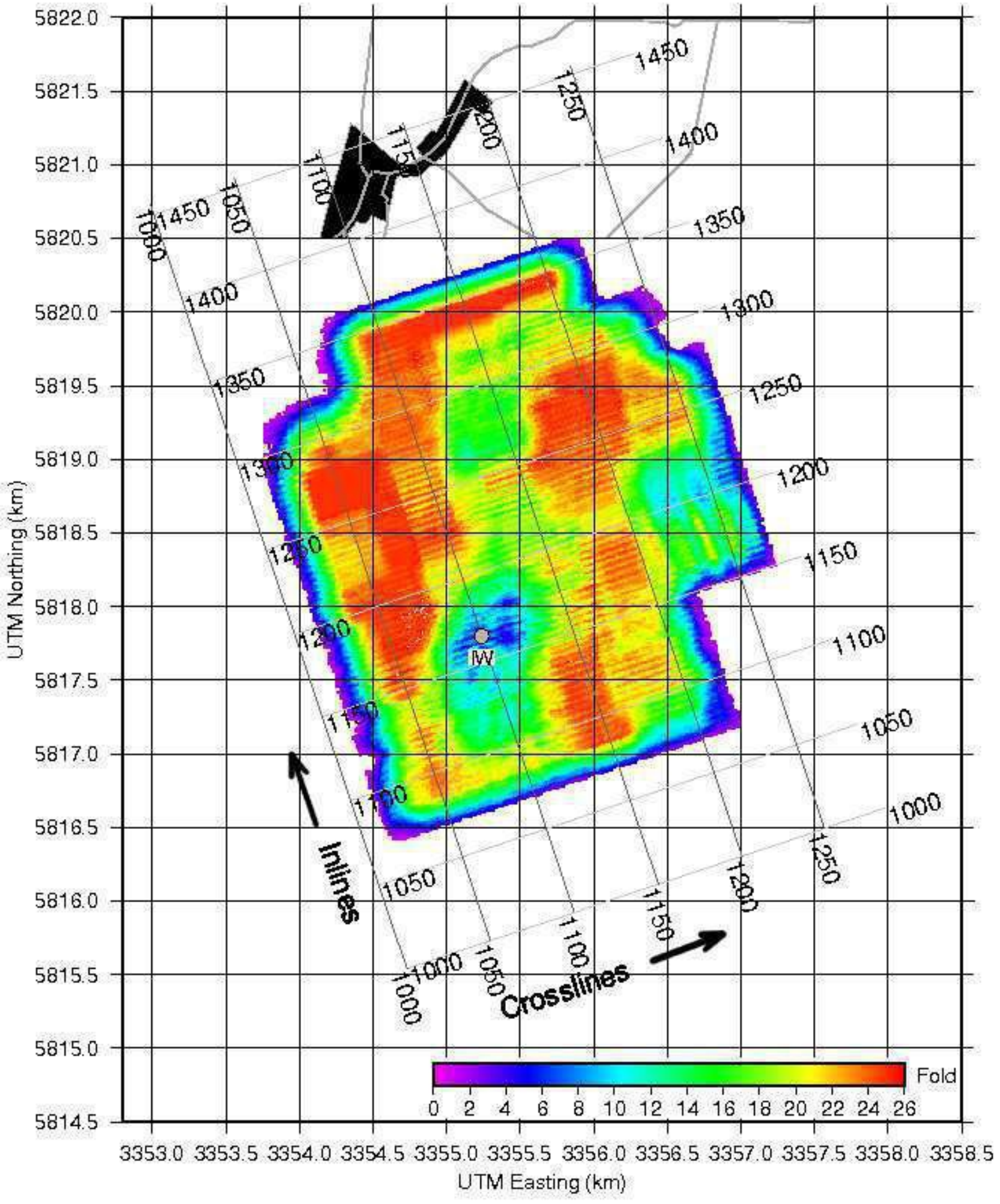
5822.0
5821.5
5821.0
5820.5
5820.0
5819.5
5819.0
5818.5
5818.0
5817.5
5817.0
5816.5
5816.0
5815.5
5815.0
5814.5
UTM Northing (km)
3353.0 3353.5 3354.0 3354.5 3355.0 3355.5 3356.0 3356.5 3357.0 3357.5 3358.0 3358.5
UTM Easting (km)
IW
Inlines
Crosslines
Fold
0 2 4 6 8 10 12 14 16 18 20 22 24 26

Figure5

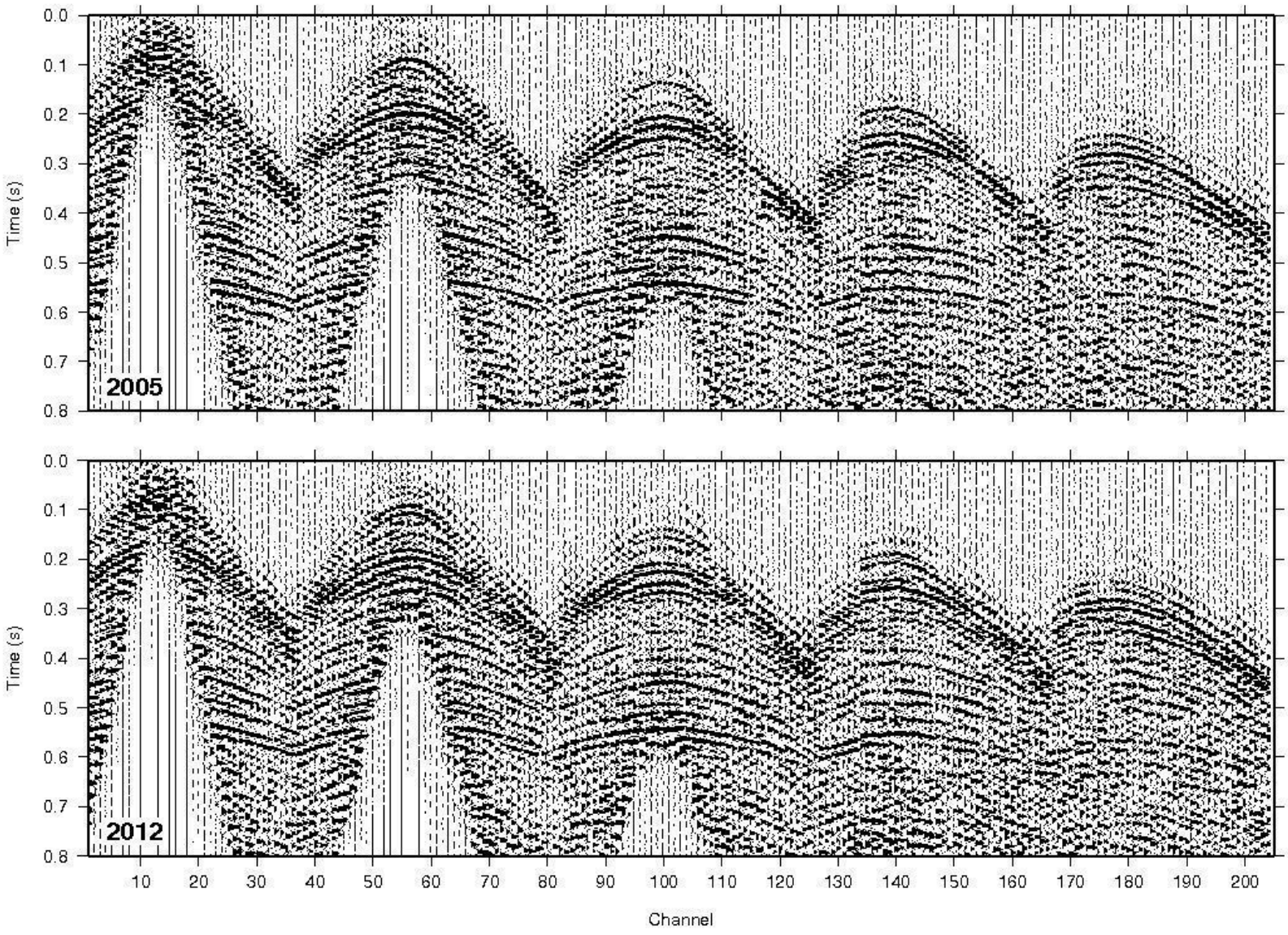
2005
2012
Time (s)
Channel
0.0
0.1
0.2
0.3
0.4
0.5
0.6
0.7
0.8
10
20
30
40
50
60
70
80
90
100
110
120
130
140
150
160
170
180
190
200

Figure6

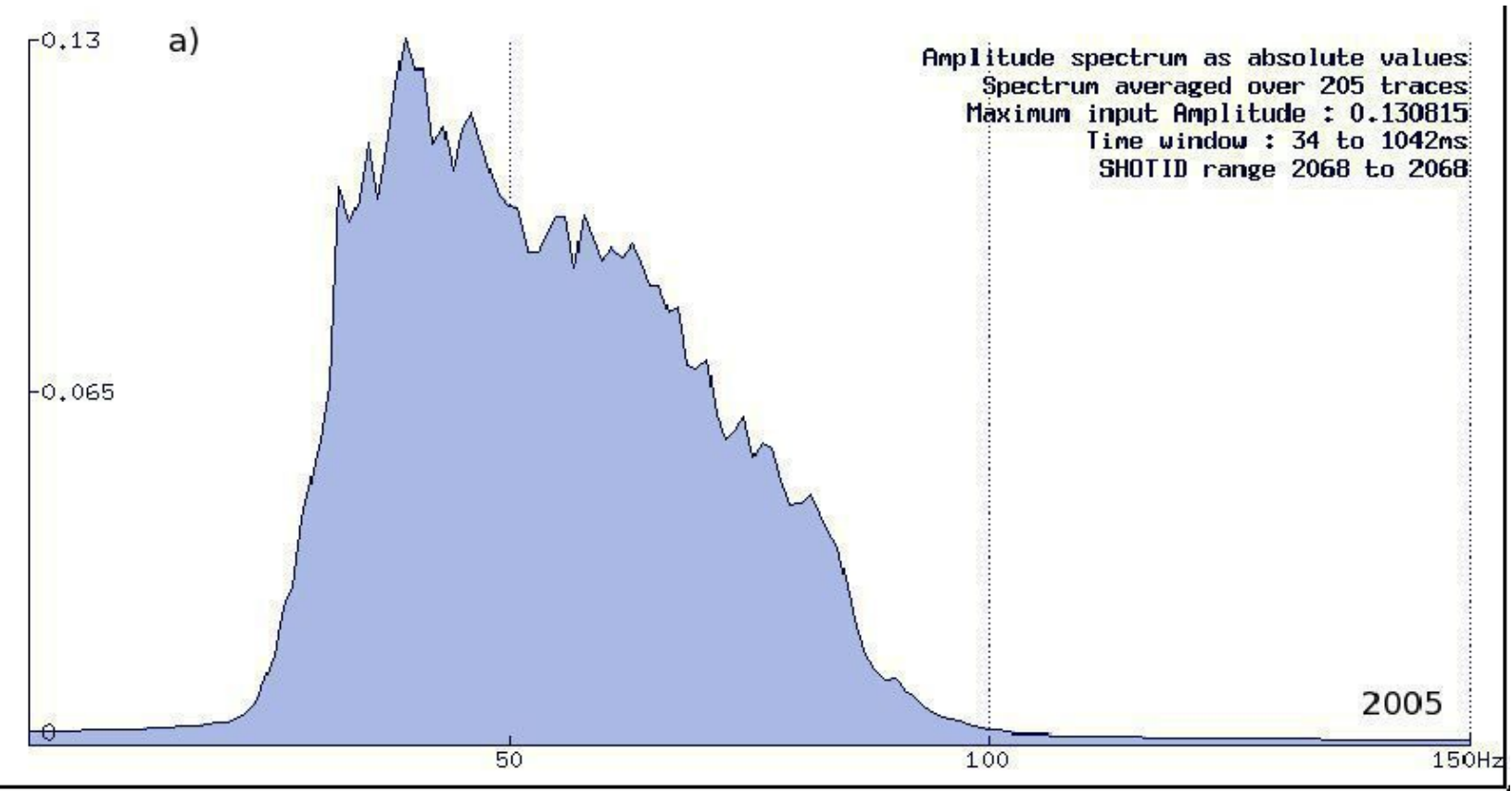
a)
0.13
0.065
0
Amplitude spectrum as absolute values
Spectrum averaged over 205 traces
Maximum input Amplitude : 0.130815
Time window : 34 to 1042ms
SHOTID range 2068 to 2068
2005
50
100
150Hz

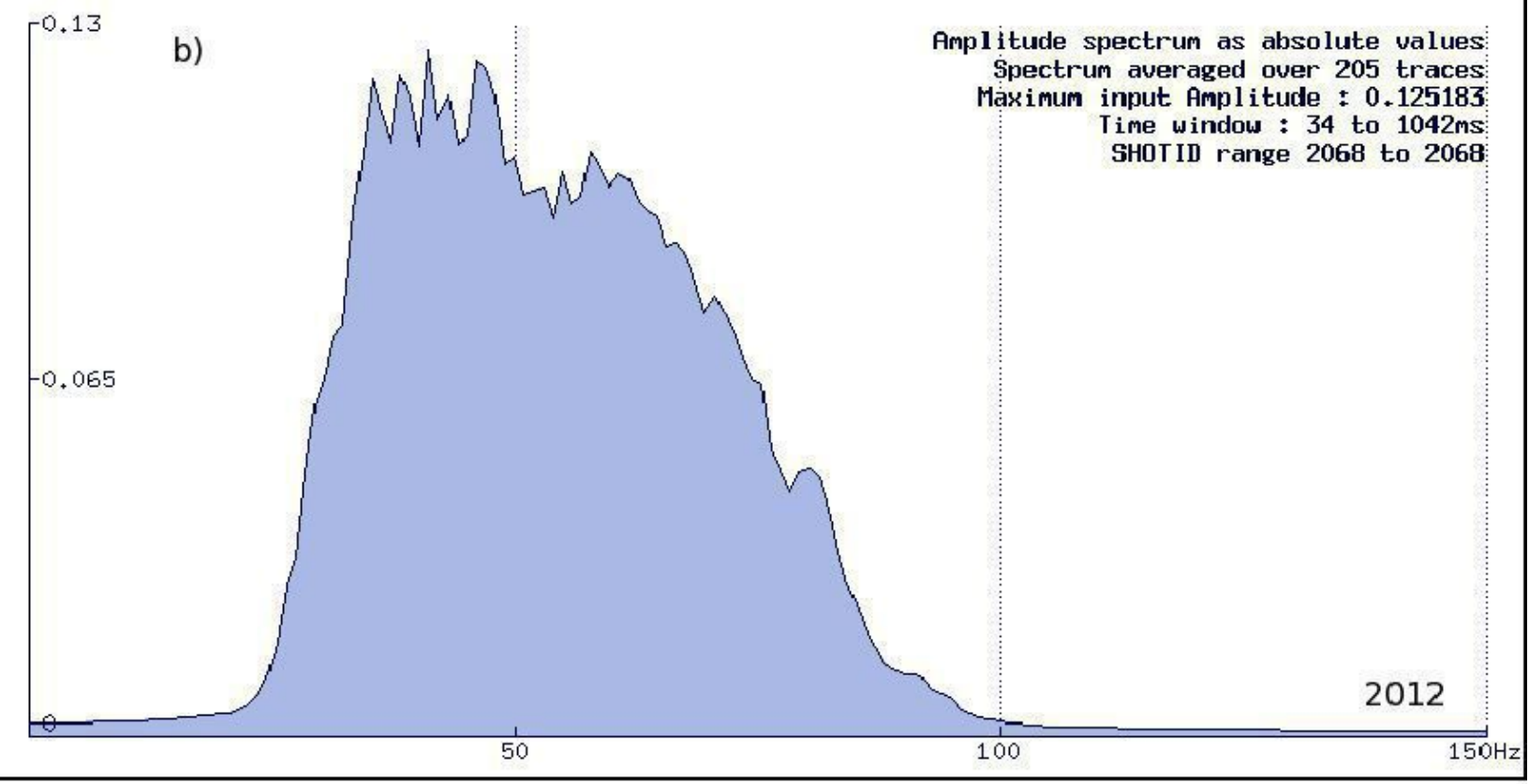
b)
0.13
0.065
0
Amplitude spectrum as absolute values
Spectrum averaged over 205 traces
Maximum input Amplitude : 0.125183
Time window : 34 to 1042ms
SHOTID range 2068 to 2068
2012
50
100
150Hz

Figure7

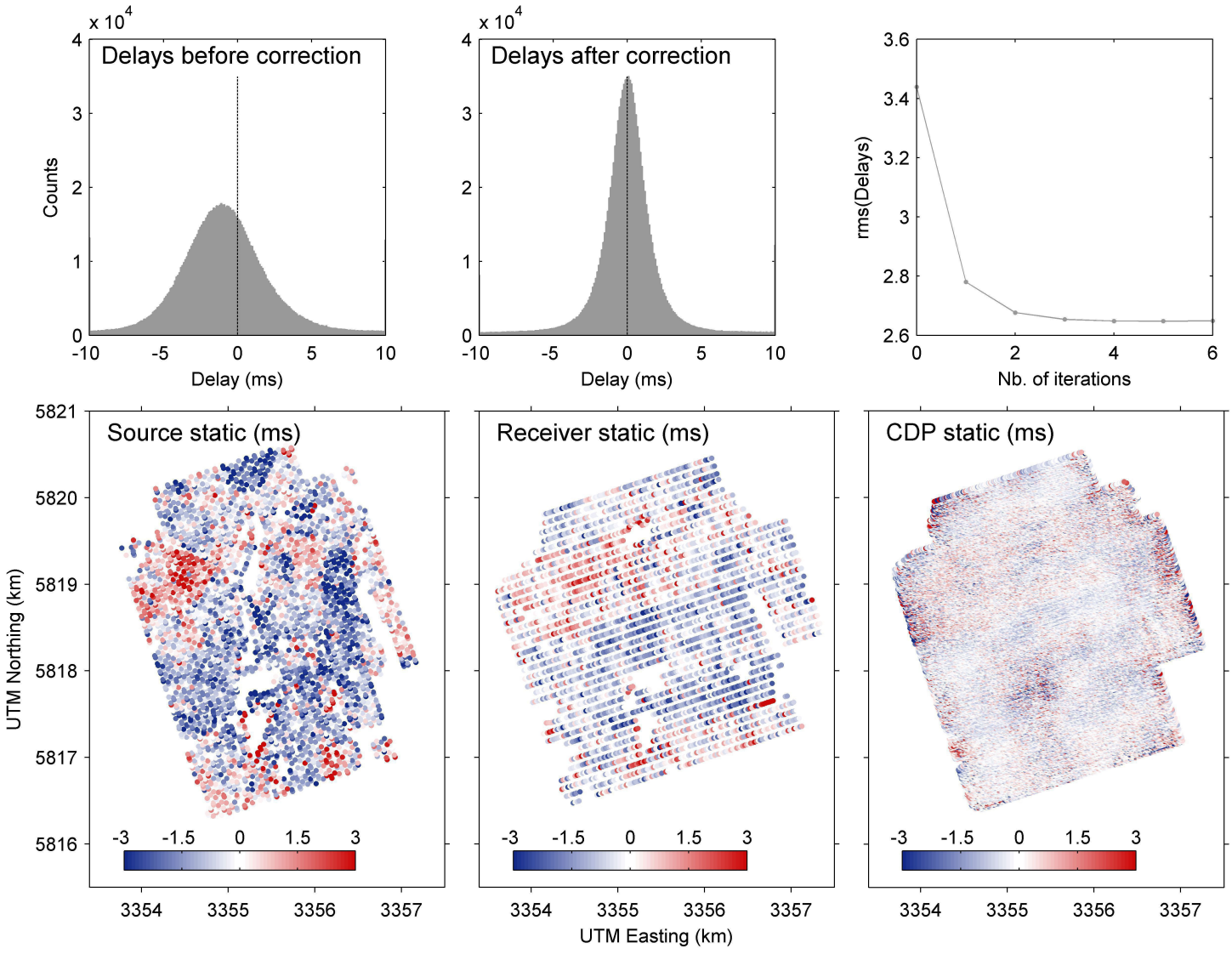
x 10^4
Delays before correction
Counts
Delay (ms)
x 10^4
Delays after correction
Delay (ms)
rms(Delays)
Nb. of iterations
Source static (ms)
Receiver static (ms)
CDP static (ms)
UTM Northing (km)
UTM Easting (km)

Figure8

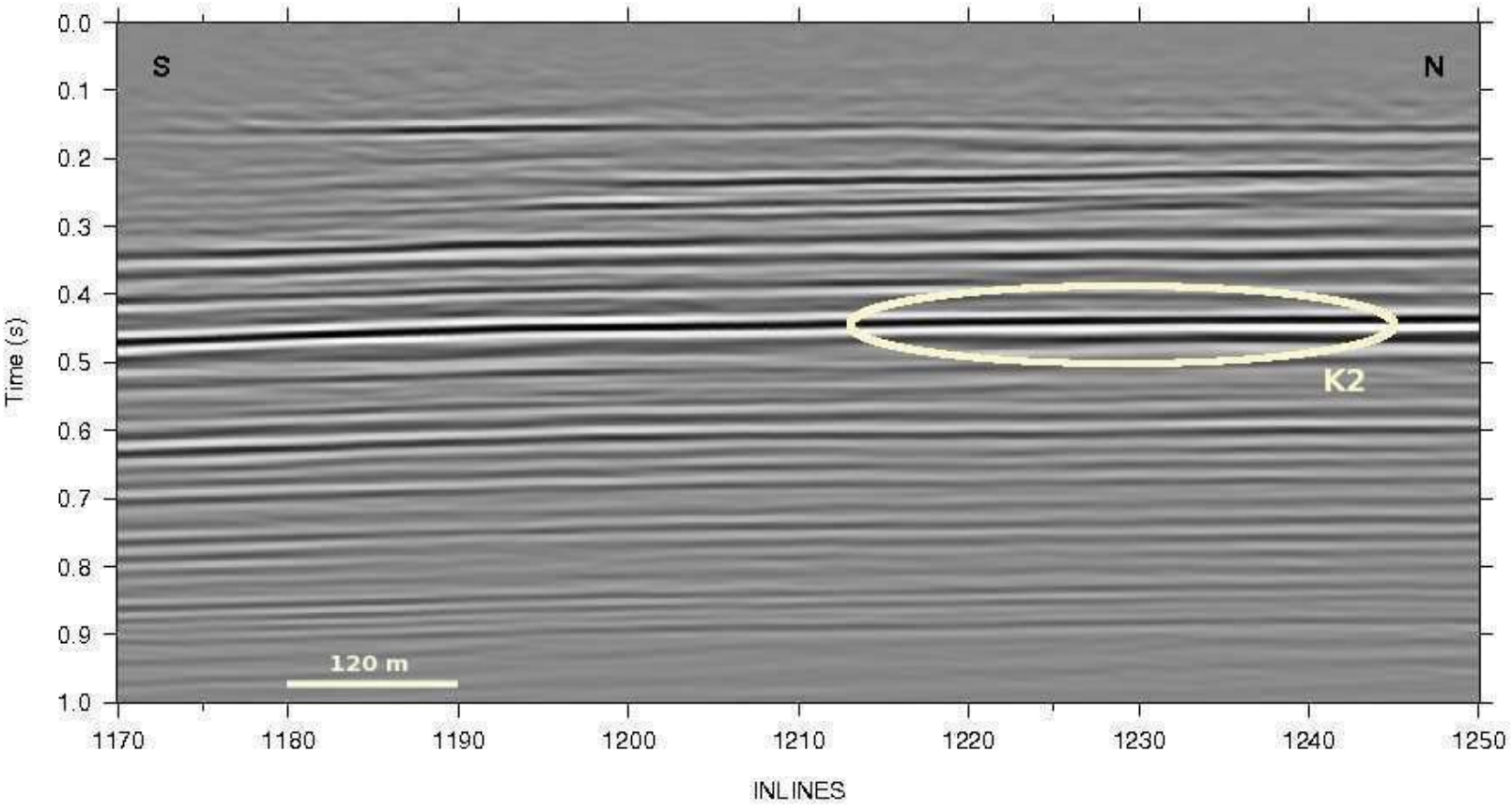
S
N
K2
120 m
Time (s)
0.0
0.1
0.2
0.3
0.4
0.5
0.6
0.7
0.8
0.9
1.0
1170
1180
1190
1200
1210
1220
1230
1240
1250
INLINES

Figure9

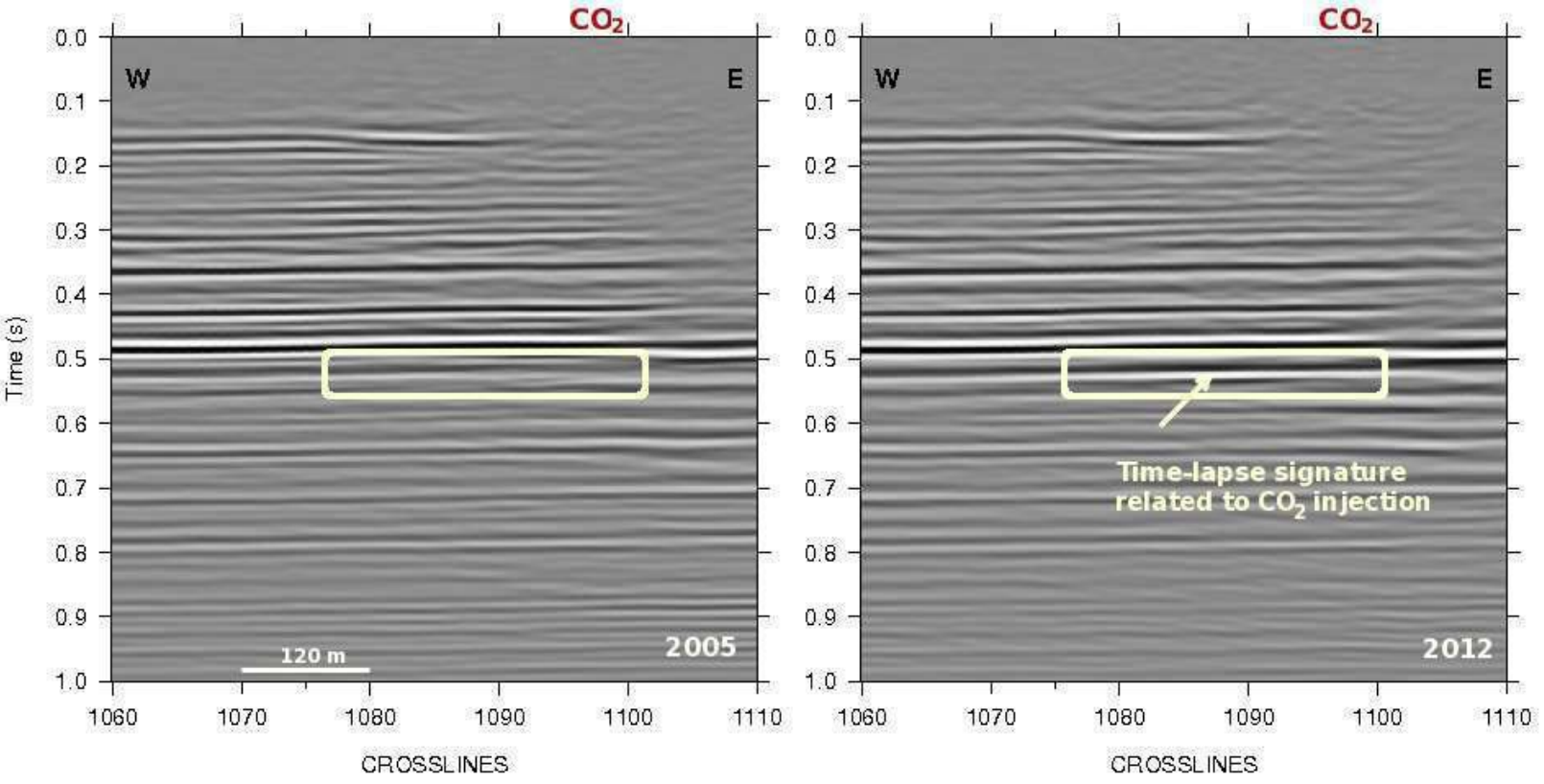
CO2
W
E
2005
120 m
CO2
W
E
2012
Time-lapse signature related to CO2 injection
Time (s)
0.0
0.1
0.2
0.3
0.4
0.5
0.6
0.7
0.8
0.9
1.0
1060
1070
1080
1090
1100
1110
CROSSLINES
CROSSLINES

Figure10

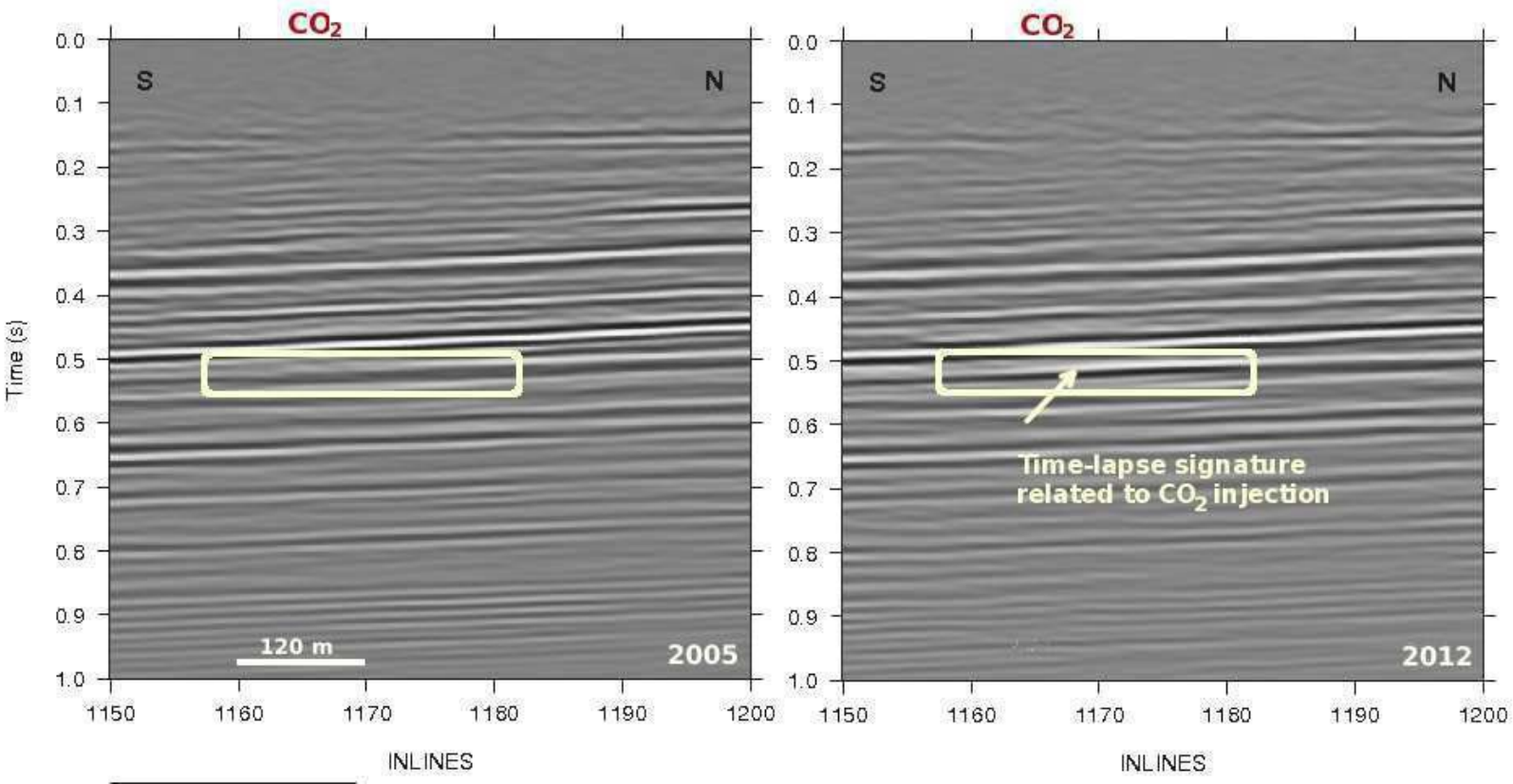
CO2
S
N
2005
120 m
CO2
S
N
2012
Time-lapse signature
related to CO2 injection
Time (s)
0.0
0.1
0.2
0.3
0.4
0.5
0.6
0.7
0.8
0.9
1.0
1150
1160
1170
1180
1190
1200
INLINES
INLINES

Figure11

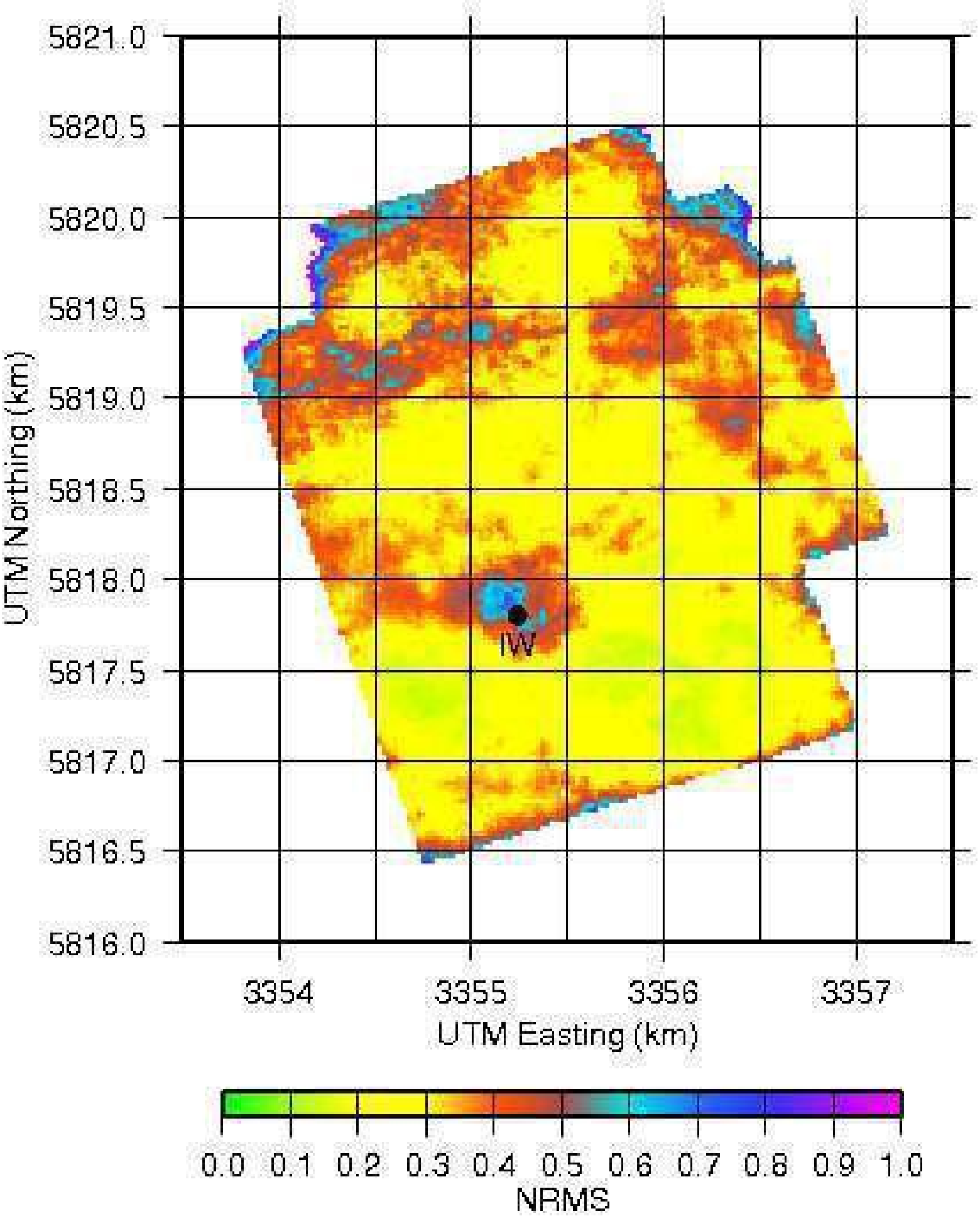
5821.0
5820.5
5820.0
5819.5
5819.0
5818.5
5818.0
5817.5
5817.0
5816.5
5816.0
UTM Northing (km)
IW
3354
3355
3356
3357
UTM Easting (km)
0.0 0.1 0.2 0.3 0.4 0.5 0.6 0.7 0.8 0.9 1.0
NRMS

Figure12

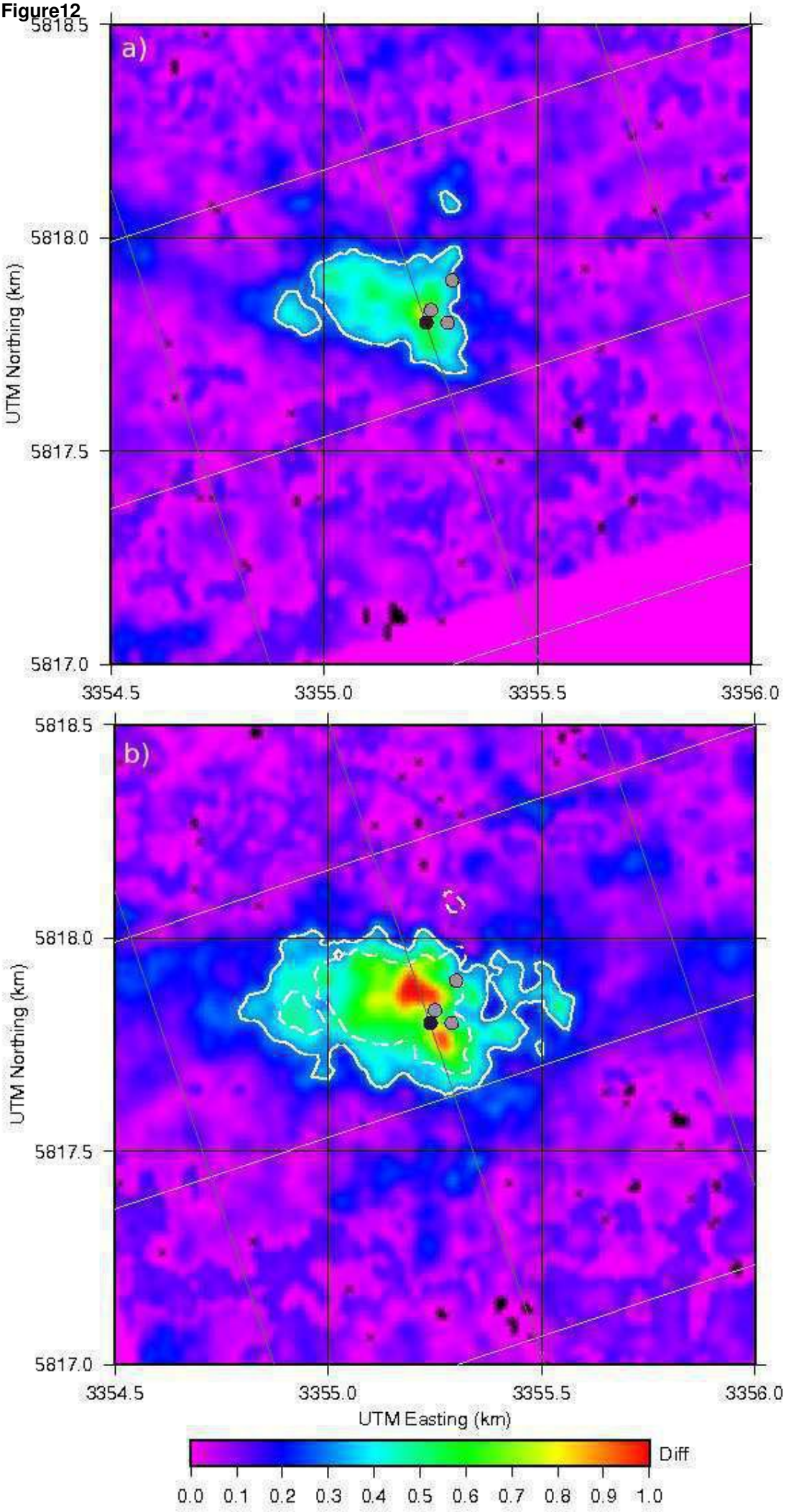
a)
b)
5818.5
5818.0
5817.5
5817.0
3354.5
3355.0
3355.5
3356.0
UTM Northing (km)
UTM Easting (km)
Diff
0.0 0.1 0.2 0.3 0.4 0.5 0.6 0.7 0.8 0.9 1.0

Figure13

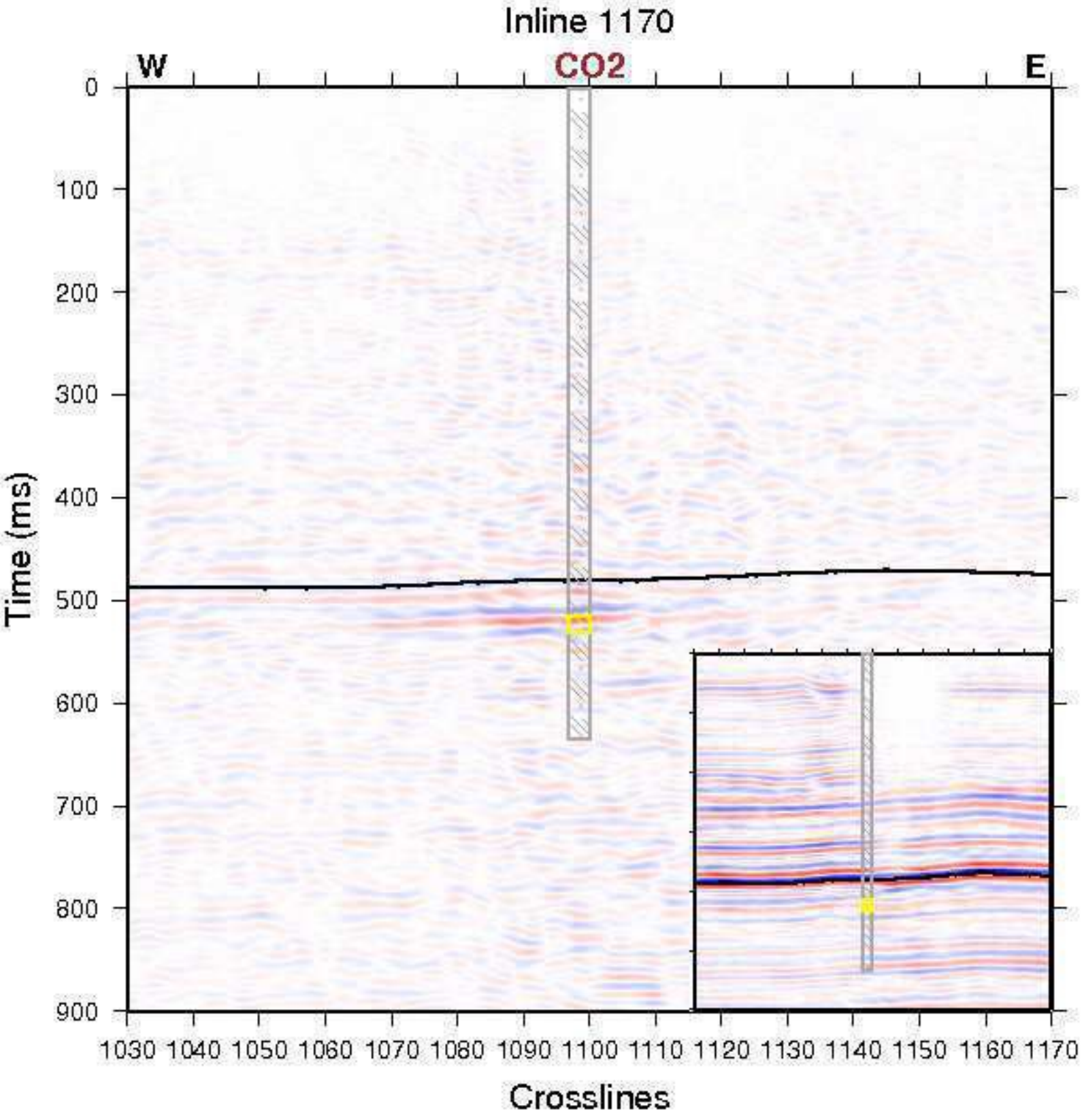
Inline 1170
W
CO2
E
0
100
200
300
400
500
600
700
800
900
Time (ms)
1030 1040 1050 1060 1070 1080 1090 1100 1110 1120 1130 1140 1150 1160 1170
Crosslines

Figure14

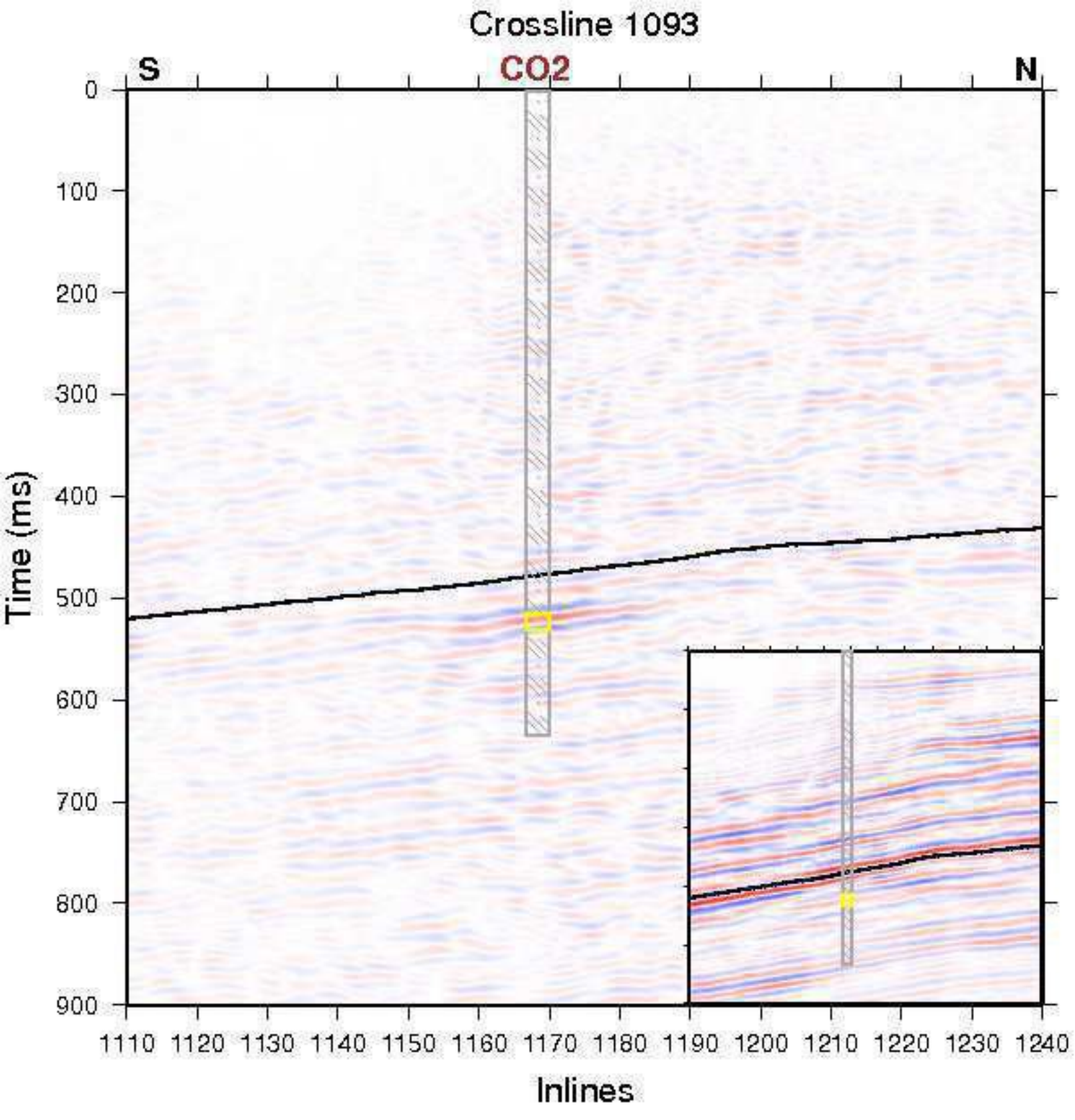
Crossline 1093
S
CO2
N
0
100
200
300
400
500
600
700
800
900
Time (ms)
1110
1120
1130
1140
1150
1160
1170
1180
1190
1200
1210
1220
1230
1240
Inlines

Figure15

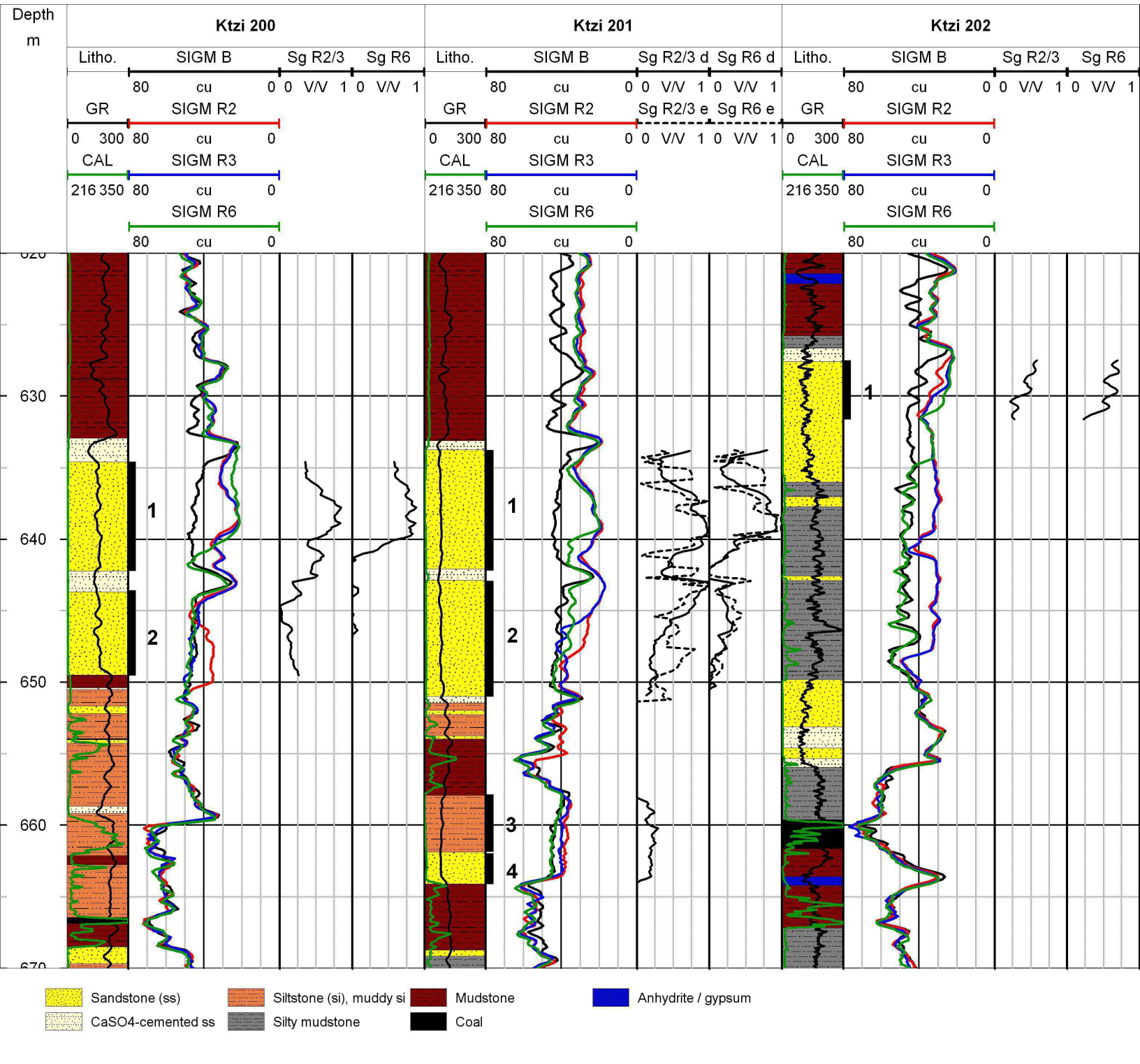
Depth
m
Ktzi 200
Ktzi 201
Ktzi 202
Litho.
SIGM B
Sg R2/3
Sg R6
Sg R2/3 d
Sg R6 d
Sg R2/3 e
Sg R6 e
GR
SIGM R2
CAL
SIGM R3
SIGM R6
80 cu 0
0 V/V 1
0 300
216 350
630
640
650
660
1
2
3
4
Sandstone (ss)
CaSO4-cemented ss
Siltstone (si), muddy si
Silty mudstone
Mudstone
Coal
Anhydrite / gypsum

Figure16

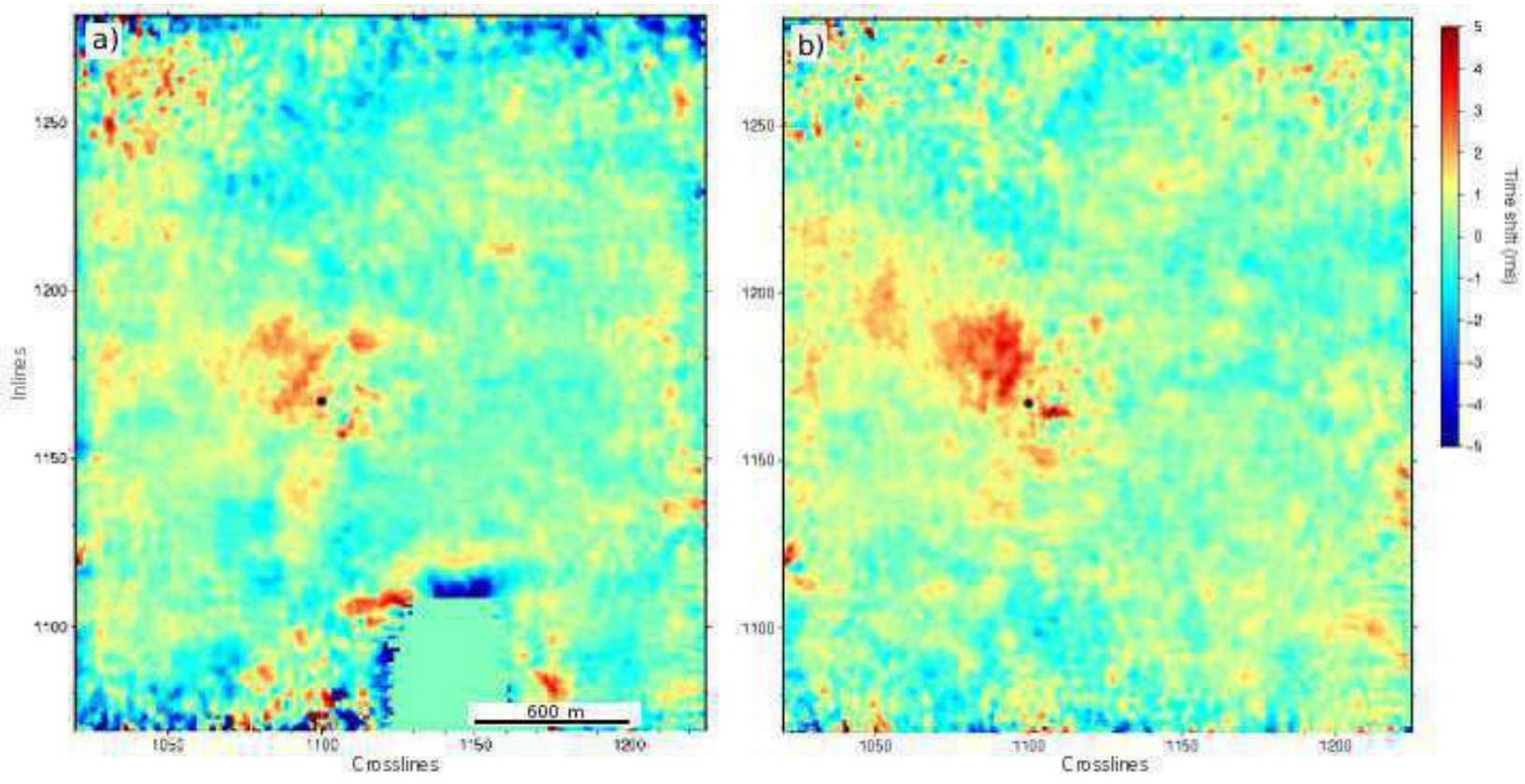
a)
b)
1250
1200
1150
1100
Inlines
1050
1100
1150
1200
Crosslines
600 m
Time shift (ms)
5
4
3
2
1
0
-1
-2
-3
-4
-5

Figure17

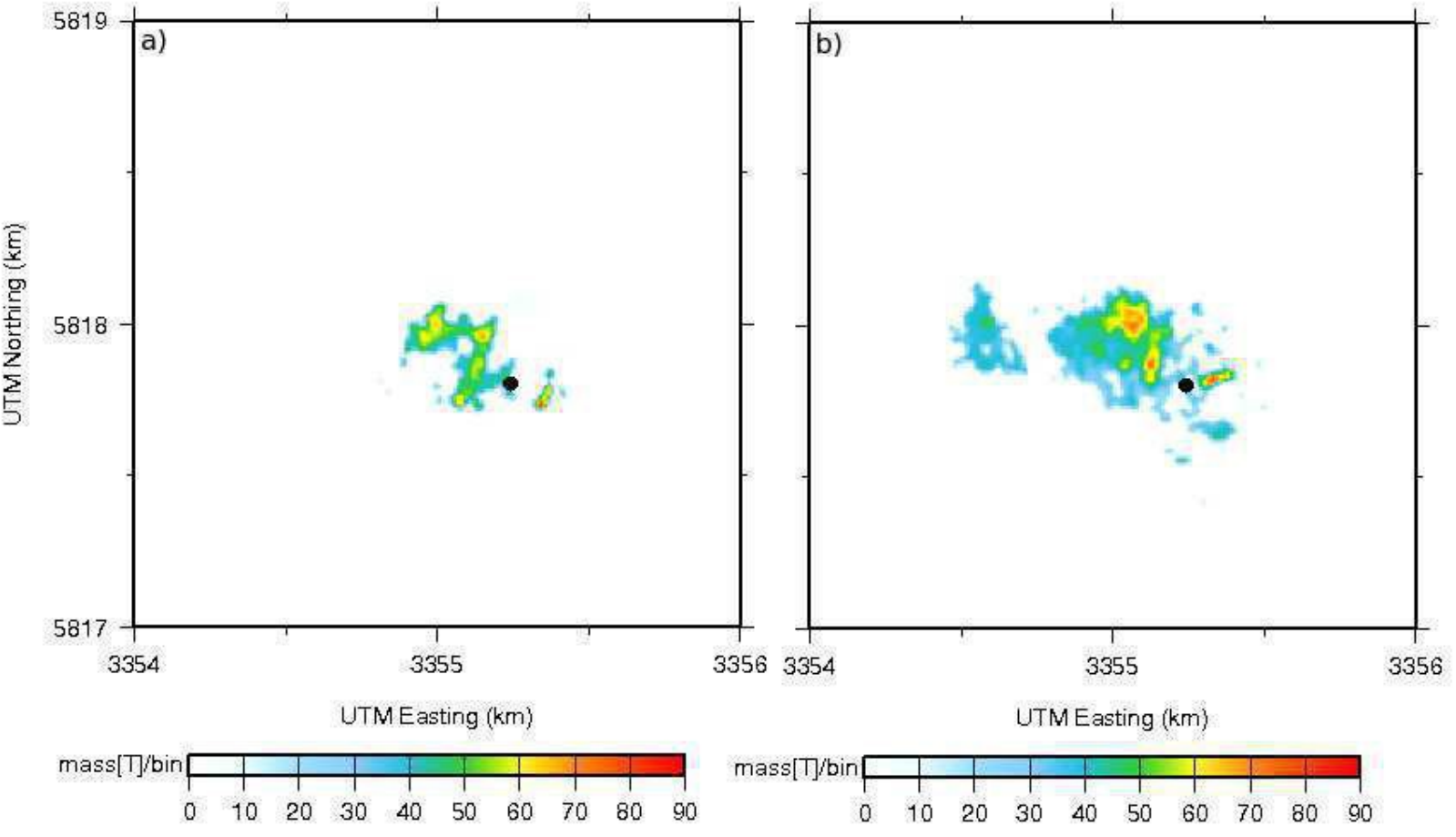
a)
b)
5819
5818
5817
UTM Northing (km)
3354
3355
3356
UTM Easting (km)
mass[T]/bin
0
10
20
30
40
50
60
70
80
90